Tau-induced increase in promoter-proximal RNA polymerase II pausing is linked to suppressed expression of long neuronal genes in a *Drosophila* tauopathy model.

Kendall Cottingham[1], Nima Goodarzi[1], David Fries[1], Geethma Lirushie[1], and Hana Hall[1,2,3*]

1 Biochemistry Department, Purdue University, West Lafayette, Indiana, USA

2 Purdue Institute for Integrative Neuroscience, Purdue University, West Lafayette, Indiana, USA

3 Purdue Institute for Cancer Research, Purdue University, West Lafayette, Indiana, USA

Correspondence:

Corresponding Author

hallh@purdue.edu

Keywords: aging, taupathy, *Drosophila*, neurodegeneration, Alzheimer's disease, promoter-proximal pausing, gene expression

Abstract

Tauopathies, including Alzheimer's disease, are age-related neurodegenerative disorders characterized by abnormal phosphorylation and buildup of microtubule-associated protein tau. Gene expression dysregulation is a key molecular feature of tauopathies, but how aging and disease interact to disrupt crucial transcriptional regulators and pathways remains largely unknown. Here, we examined how pathological tau affects gene expression programs in age-related neurodegenerative disease using a well-established *Drosophila melanogaster* tauopathy model with neuronal expression of the toxic human tau^{R406W}. Transcriptomic analysis of tau-expressing fly heads showed a preferential downregulation of long neuronal genes with long introns. Notably, we found that these downregulated genes in the tauopathy model are marked by increased accumulation of initiating RNA polymerase II (RNAP II) near the transcription start site and reduced elongating RNAP II within gene bodies, indicating a problem with the transition from initiation to elongation. By calculating an RNAP II Pause Index (PI) for each gene, we identified a strong link between promoter-proximal RNAP II stalling, gene expression

deficits, and gene length in the tauopathy model. Overall, we have uncovered the genomic and transcriptomic features of tau-dependent downregulated genes and identified increased RNAP II promoter-proximal stalling as a significant mechanism of transcription stress in tauopathy.

1. Introduction

Tauopathies are a diverse group of age-related neurodegenerative disorders characterized by the abnormal accumulation of tau, a microtubule-associated protein essential for microtubule assembly and stability (Black et al., 1996; Ramírez et al., 1999). The presence of intracellular neurofibrillary tangles composed of hyperphosphorylated tau is a key pathological feature of Alzheimer's disease (AD) and frontotemporal dementia with parkinsonism linked to chromosome 17 (FTDP-17) (Hutton, 2000). Mutations in the microtubule-associated protein tau (MAPT) gene that affect microtubule binding, phosphorylation, or aggregation are responsible for most FTDP-17 cases (Goedert and Spillantini, 2000). FTDP-17 primarily affects the frontal and temporal lobes of the brain, leading to progressive changes in behavior and personality, communication difficulties, and impairments in memory and motor skills.

Although tau is involved in the development of various neurodegenerative diseases, the cellular mechanisms that cause neuronal dysfunction and death are still not well understood. Understanding the pathways that promote tauopathy progression, especially in the context of aging—which is the main risk factor for the disease—is crucial for deepening our knowledge of the molecular basis of tau-driven neurodegeneration (Niccoli and Partridge, 2012). Gene expression is increasingly recognized as a key factor in the development of tauopathies in both mouse models and human patients (Miller et al., 2008, 2010; Tan et al., 2021). During aging, existing transcriptional programs undergo widespread changes, driven by factors such as accumulated DNA damage and epigenetic modifications (López-Otín et al., 2023). These changes are thought to cause many of the physical signs of aging and age-related diseases. Previously, we showed that long, highly expressed genes encoding proteins with neuronal functions exhibit reduced expression in aging neurons (Hall et al., 2017). Later studies have also supported a connection between gene structure, transcription levels, and cellular function across different tissues and organisms, in aging and neurodegenerative disease contexts (Barbash and Sakmar, 2017; Lopes et al., 2021; Jauregui-Lozano et al., 2022; Stoeger et al., 2022; Debès et al., 2023; Gyenis et al., 2023). However, how aging and disease interact to alter the cellular environment and affect key transcriptional regulators that control gene expression remains largely unknown.

To investigate how tau affects gene expression programs in age-related neurodegenerative disease, we used a well-established *Drosophila melanogaster* tauopathy model with neuronal expression of human tau carrying the R406W mutation. Using steady-state RNA sequencing (RNA-seq), we characterized the age- and tau-dependent transcriptome in tauopathy flies. In tau transgenic flies, we observed a preferential downregulation of long genes characterized by long introns that encode factors essential for neuronal structure and function. Additionally, using the RNA polymerase II (RNAP II)-targeted Cleavage Under Targets and Release Using Nuclease (CUT&RUN) approach, we analyzed tau-dependent transcription dynamics. Downregulation of long genes was strongly linked to increased RNAP II stalling near the transcription start site (TSS) and decreased RNAP II occupancy along the gene body in the tauopathy model, suggesting that impaired promoter-proximal pause release is a likely mechanism behind their reduced expression. Overall, our results reveal the transcriptional dynamics and genomic features of genes dysregulated in tauopathy and their relationship to progressive, age-related neurodegeneration. Importantly, promoter-proximal RNAP II stalling emerged as a key characteristic of long, downregulated neuronal genes, implicating tau-dependent dysregulation of the transition from transcription initiation to productive elongation as a possible molecular driver of transcriptional stress in tauopathy.

2. Materials and Methods

2.1 *Drosophila* Stocks and Maintenance

The following strains used in this study were from Bloomington *Drosophila* Stock Center: elav>Gal4 (BDSC #8765), UAS-lacZ (BDSC #8529), UAS-tau (BDSC #78851). The UAS-TAU^{R406W} strain was a gift from Mel Feany (Wittmann et al., 2001). Flies were maintained under a 12:12-hour light: dark cycle at 25°C on standard fly food. For aging experiments, flies were collected within three days post-eclosion and transferred to fresh food every two days.

2.2 Optic Neutralization

86 Optic neutralization was performed as previously described (Stegeman et al., 2018). Briefly, 10
87 male flies per genotype were aged to the designated time point, anesthetized on a CO_2 pad,
88 and mounted to glass slides using clear nail polish as adhesive. Live rhabdomeres were imaged
89 using brightfield light microscopy at 20x magnification. For each genotype and time point, at
90 least 70 rhabdomeres were assessed. Retinal degeneration was quantified in a blinded manner
91 and expressed as the percentage of lost rhabdomeres relative to the total number of
92 rhabdomeres.

93

94 **2.3 Climbing Assay**

95 Climbing assays were performed using groups of 25 male flies per genotype. Flies were sorted
96 into vials and allowed to recover for 24 hours following anesthesia. The next day, flies were
97 gently tapped into a 100 ml glass graduated cylinder and acclimated for 2 minutes. The cylinder
98 was then tapped firmly and swiftly three times to bring the flies to the bottom. Flies were given
99 10 seconds to climb, and the number of flies above a 5 cm mark was recorded. Each biological
100 replicate consisted of three technical trials, with a one-minute rest between tests. For each
101 genotype, 6-12 biological replicates (a total number of 150-300 flies) were assessed.

102

103 **2.4 Western Blotting**

104 Western blot analysis was performed using 40 µg of whole-cell protein extract from 25 fly
105 heads per genotype. Heads were manually homogenized in cell lysis buffer (50 mM Tris-HCl, pH
106 8.0, 150mM NaCl, and 1% NP-40). Antibodies used for detection are listed in Supplemental Data
107 2.

108

109 **2.5 RNA Extraction, Reverse Transcription-quantitative PCR (qPCR), and RNA-seq**

110 Total RNA was extracted from 20-25 fly heads per genotype by mechanical homogenization in
111 TRIzol reagent (Thermo Fisher, #15596018), followed by phenol/chloroform extraction and
112 ethanol precipitation using standard protocols. cDNA was synthesized from 300-400 ng of total

113 RNA using Episcript RNaseH Reverse Transcriptase (Biosearch Technologies, #ERT12925K-ENZ)
114 with random hexamer primers (IDT). Quantitative PCR (qPCR) was performed using PR1MA
115 qMAX Green 2X qPCR mix (Midsci, #PR2000-N-5000) on a CFX Connect Real-Time System
116 (BioRad) according to the manufacturer's instructions. Relative gene expression was normalized
117 to the geometric mean of two reference genes in accordance with MIQE guidelines (Bustin et
118 al., 2009). Primer sequences are provided in Supplemental Data 2.

119 For RNA-seq, extracted RNA was treated with DNase I (Roche, #04716728001) to remove
120 genomic DNA according to the manufacturer's protocol. Purified RNA was quantified using the
121 Qubit RNA HS Assay Kit (ThermoFisher, #Q32852). cDNA libraries were prepared from 250 ng of
122 RNA using the Universal Plus™ Total RNA-Seq Library Preparation Kit, incorporating *Drosophila*-
123 specific anyDeplete technology for rRNA depletion (Tecan, #9156). Libraries were pooled and
124 sequenced using paired-end 150 bp reads in a single lane on an Illumina Novaseq X Plus
125 platform.

126

127 **2.6 Bioinformatic Analysis of RNA-seq Data**

128 Bioinformatic analysis of RNA sequencing data was performed as previously described
129 (Jauregui-Lozano et al., 2022) with minor adjustments. Raw reads were trimmed using
130 Trimmomatic (Bolger et al., 2014) to remove adapter sequences and low-quality bases. Cleaned
131 reads were then quantified using Salmon (Patro et al., 2017) against a custom reference
132 transcriptome built from *Drosophila melanogaster* (BDGP6.54) cDNA sequences, with the
133 addition of *Homo sapiens* MAPT transcript information extracted from the GRCh38 cDNA
134 reference. The resulting transcript-level counts were summarized to gene level and analyzed in
135 R using the DESeq2 (Love et al., 2014) package for differential expression analysis. Cut-offs for
136 differential gene expression were adjusted to a p-value < 0.05 and $|\text{fold change}| > 1.5$ unless
137 otherwise stated. For comparisons between differential expression groups, statistical analysis
138 was performed using ANOVA followed by a Tukey HSD post-hoc test. Gene Ontology (GO)
139 enrichment analysis of significantly differentially expressed genes was performed using
140 clusterProfiler (Yu et al., 2012).

141

142 **2.7 CUT&RUN**

143 CUT&RUN was performed using the EpiCypher CUTANA protocol with modifications for nuclei
144 isolation from fly head tissue. Briefly, 100 fly heads were homogenized in 1 mL of Nuclear
145 Extraction Buffer (20 mM HEPES, pH 7.9, 10 mM KCl, 0.1% Triton-X, 20% glycerol, 0.5 mM
146 spermidine, 1× protease inhibitor) using a 1 mL Dounce homogenizer. Homogenization
147 comprised 7 loose pestle strokes, a 5-minute ice incubation, followed by 7 loose and 12 tight
148 pestle strokes. The homogenate was filtered through a 70 µm cell strainer, and 100 µL of nuclei
149 was incubated with 11 µL of activated ConA beads per reaction. Targeted MNase cleavage was
150 directed by antibodies listed in Supplemental Data 2. DNA was purified using the Zymo ChIP
151 DNA Clean & Concentrator Kit (#D5205), and libraries were prepared with the EpiCypher
152 CUTANA Library Preparation Kit (#14-1001). The libraries were pooled and sequenced in a
153 single lane using paired-end 150-bp reads on an Illumina Novaseq X Plus platform.

154

155 **2.8 Bioinformatics Analysis of CUT&RUN Data**

156 Raw paired-end reads were trimmed and filtered for adapter sequences and low-quality bases
157 using Fastp (Chen et al., 2018). Cleaned reads were aligned to the *Drosophila*
158 *melanogaster* BDGP6.46 reference genome (annotation release 113) using Bowtie2 (Langmead
159 and Salzberg, 2012) with end-to-end, sensitive parameters. The resulting BAM files were sorted
160 with SAMtools and duplicate reads removed with Picard MarkDuplicates. Peak calling was
161 performed using MACS3 (Zhang et al., 2008) with broad peak settings. The resulting pileup
162 bedGraph files were normalized to counts per million (CPM) based on the total number of
163 mapped reads and converted to BigWig format using bedGraphToBigWig from the UCSC
164 Genome Toolkit. Normalized BigWig files were used to visualize metagene and signal profiles
165 with deepTools (Ramírez et al., 2016), using the computeMatrix and plotProfile functions. For
166 peak analysis, consensus peaks (defined as peaks present in at least three out of four biological
167 replicates per condition) were identified using bedtools multiinter (Quinlan and Hall, 2010).

The RNAP II pause index (PI) is a gene-specific quantitative measure that assesses tau-dependent changes in promoter-proximal pausing relative to controls. Specifically, the Ser5-P pause index was calculated as the ratio of promoter Ser5-P RNAP II signal (transcription start site [TSS] ± 250 bp) to gene body Ser5-P RNAP II signal (+500 bp from the TSS to –500 bp from the transcription end site [TES]). Given the defined coordinates for promoter and gene body regions, a minimum gene length cutoff of 1500 bp was applied. Total Ser2-P was calculated independently as the average elongating RNAP II signal across the defined gene body region, serving as a direct measure of productive elongation. To determine tau-dependent differences in pause status, log2 fold changes of both the Ser5-P pause index and total Ser2-P signal were computed between tau-expressing and control flies on a per-gene basis. Overall, the RNAP II PI can capture relative changes in promoter-proximal RNAP II accumulation and relative levels of the elongating RNAP II signal in the tauopathy model. RNAP II PI can be mathematically defined as:

$$\log\left(\frac{\left(\frac{Ser5P\ Promoter}{Ser5P\ Gene\ Body}\right)^{Tau}}{\left(\frac{Ser5P\ Promoter}{Ser5P\ Gene\ Body}\right)^{Ctrl}}\right) - \log\left(\frac{\left(Ser2P\ Total\right)^{Tau}}{\left(Ser2P\ Total\right)^{Ctrl}}\right) =$$

$$RNAP\ II\ Pause\ Index\ (PI)$$

185 **3. Results**

186 **3.1 Tau^{R406W} induces progressive, age-related neurodegeneration in a *Drosophila* tauopathy**
187 **model.**

188 The tau R406W mutation, linked to FTDP-17 (Hutton, 2000; Nakamura et al., 2019), occurs at a
189 conserved residue of exon 13 within the C-terminal domain, affecting all tau isoforms (Figure
190 1A) (Hong et al., 1998). Importantly, this mutant form of tau has structural and biochemical
191 properties similar to those found in AD and FTDP-17 patients (Hutton, 2000). Tau R406W
192 promotes hyperphosphorylation of tau, impairs its ability to bind microtubules, and increases
193 neuronal vulnerability to apoptotic stress, thereby contributing to neuronal cell loss observed in
194 tauopathy (Krishnamurthy and Johnson, 2004). In mouse models, tau R406W causes tau
195 hyperphosphorylation and filament aggregation, disrupting axonal transport in affected
196 neurons (Tatebayashi et al., 2002; Zhang et al., 2004; Ikeda et al., 2005). In *Drosophila*, pan-
197 neuronal expression of transgenic human tau R406W (elav>htau^{R406W}) (Figure S1A-C)
198 reproduces key features of human tauopathies, including DNA damage (Frost et al., 2014),
199 impaired locomotion (Merlo et al., 2014), and neuronal cell death (Wittmann et al., 2001).
200 Using optic neutralization of the fly eye, we demonstrated that pan-neuronal expression of
201 toxic htau R406W results in significant photoreceptor neuron loss starting in young, 10-day-old
202 flies, which markedly worsens by middle age, 20 days after eclosion (Figure 1B, C, Figure S1D).
203 In contrast, neuronal expression of wild-type human tau (WT-htau) does not cause retinal
204 degeneration even in older flies, 40 days post-eclosion (Figure S1E). Notably, no rhabdomere
205 loss was observed in 2-day-old early adult htau^{R406W} transgenic flies, indicating that tau-induced
206 neurodegeneration is age-dependent and not due to retinal developmental defects. Similarly,
207 progressive adult-onset brain vacuolization, a well-established marker of neurodegeneration in
208 flies, has also been reported in this model (Wittmann et al., 2001).

209 To further assess age-related neurodegeneration in tau transgenic flies, we examined
210 behavioral indicators of neuronal function. We carried out longitudinal climbing assays on
211 htau^{R406W} transgenic flies and age-matched controls (no tau expression) to assess locomotion.
212 Control flies maintained a high, consistent climbing score across different ages. In contrast,

213 tau^{R406W} transgenic flies showed a 25% decrease in climbing ability at day 2 post-eclosion
214 compared to controls (Figure 1D). This early-adulthood climbing-deficit phenotype suggests
215 that htauR406W expression during development impairs neuronal function without affecting
216 overall organization or survival. By day 10, htau^{R406W} transgenic flies demonstrated a 50%
217 reduction in climbing ability relative to controls, with this decline progressing to a 70%
218 reduction by day 20 (Figure 1D). The htau^{R406W} transgenic line, hereafter referred to as tau
219 transgenic flies, exhibits quantifiable neurodegeneration early in life—before significant survival
220 declines—making it an ideal model for studying mechanisms of tau-induced neuropathology
221 (Wittmann et al., 2001). Additionally, they mimic the progressive, age-related
222 neurodegenerative features seen in human tauopathies, highlighting their relevance as a
223 *Drosophila* model of dementia (Creekmore et al., 2024).

224 **Figure 1 Legend:**

225 **(A)** Schematic of the human tau transgene isoform showing defined domains and the location
226 of the R406W mutation. **(B)** Schematic illustrating the ageing time points used for phenotypic
227 analysis. **(C)** Boxplot quantification of retinal degeneration in aged control (*elav>lacZ*) and tau
228 (*elav>htau^{R406W}*) flies. Rhabdomeres of 10 individual ommatidia per fly (n=10 male flies) were
229 assessed. Retinal degeneration scores were calculated blindly as the ratio of the number of lost
230 rhabdomeres to the total number of rhabdomeres, indicating photoreceptor cell death. **(D)**
231 Boxplots showing the climbing ability of aged control (*Cyo/ htau^{R406W}*) and tau (*elav>htau^{R406W}*)
232 flies. 6-12 replicates of 25 male flies were assessed for each genotype. Student's t-test was used
233 to determine statistical significance between genotypes at each time point (**** $p < 0.001$, **p
234 < 0.01, *$p < 0.05$, NS/ns not significant).

235 **Supplementary Figure 1 Legend:**

236 **(A)** A diagram illustrating a genetic approach to create a *Drosophila* tauopathy model using pan-
237 neuronal *elav-Gal4*-driven expression of the toxic hTau^{R406W}. Relative htau RNA **(B)** and protein
238 **(C)** levels in 10-day-old transgenic flies. n=3 replicates of 25 male flies per genotype. **(D)** Left:
239 Schematic of the *Drosophila* compound eye showing a single ommatidium enlarged to display
240 photoreceptor neurons (R1-7) with rhabdomeres (red circles). Right: Representative images

241 showing the loss of rhabdomeres in photoreceptor neurons (indicated by yellow arrowheads) in
242 tau (*elav>htau*^{R406W}) flies. **(E)** Boxplot quantification of retinal degeneration observed in aged
243 flies expressing WT-htau. Student's t-test was used to determine statistical significance
244 between genotypes at each time point (NS/ns not significant).

245

246 **3.2 Toxic tau expression drives dysregulation of neuronal, immune response, and cell cycle**
247 **genes.**

248 Accumulation of tau in *Drosophila* and mouse models, as well as human brain tissue, leads to
249 global chromatin relaxation and altered gene expression profiles, contributing to the
250 development of neurodegenerative symptoms (Frost et al., 2014). Comprehensive
251 transcriptomic analyses of human post-mortem brain tissue from individuals with AD and
252 related tauopathies reveal distinct gene expression changes that correlate with cognitive and
253 physical impairments (Mostafavi et al., 2018; Wan et al., 2020). Similarly, transcriptome
254 profiling across various tau transgenic mouse models has revealed consistent transcriptomic
255 alterations, including decreased expression of genes encoding synaptic proteins and increased
256 expression of immune-response genes (Gjoneska et al., 2015; Kim et al., 2019). Thus, we sought
257 to determine whether the tau-associated neurodegeneration observed in our *Drosophila*
258 tauopathy model was accompanied by significant and clinically relevant alterations in canonical
259 gene expression.

260 We conducted longitudinal RNA-seq using RNA extracted from the heads of control and tau
261 transgenic flies at 2, 10, and 20 days post-eclosion (Supplemental Data 1). Three independent
262 biological replicates, each comprising 20 male flies, were analyzed for each genotype and time
263 point, except for a single discordant day 2 tauopathy fly sample, which was excluded from
264 further analysis (Figure S2A and S2B). Principal component analysis (PCA) of the normalized
265 transcript counts revealed that age accounted for 51% of the total variance across all samples,
266 while tau expression contributed 18% (Figure S2A). Overall, the greatest variability in gene
267 expression was observed among day 2 samples, likely reflecting dynamic transcriptional
268 changes associated with the transition to adulthood. In contrast, samples from 10- and 20-day-

269 old flies showed distinct genotype-specific clustering, indicating that tau expression is the
270 primary driver of transcriptomic differences at these later stages (Figure S2B).

271 Longitudinal transcriptomic analysis revealed the greatest number of perturbations at day 10,
272 with 1,640 differentially expressed genes (DEGs) identified in tau-expressing flies compared to
273 controls (Figure 2A). In contrast, 704 and 805 DEGs were identified at days 2 and 20,
274 respectively (Figure 2B 2C). Of all DEGs, 364 were consistently dysregulated across all three age-
275 time points (Figure 2D), and these were enriched for gene ontology (GO) terms related to
276 synaptic transmission and nervous system processes (Supplemental Data 1). This group includes
277 9 of the 10 genes encoding members of the synaptic nicotinic acetylcholine receptor (*nAChR*), a
278 ligand-gated ion channel that regulates neuronal membrane potential. Decreases in human
279 homologues of acetylcholine transporters and receptors yield cholinergic neuronal dysfunction
280 in aging and AD (Nyakas et al., 2011). Consistently downregulated genes also included *Syt1* and
281 *Tomosyn,* whose human orthologs, SYT1 and STXBP5, are significantly downregulated in
282 postmortem AD brain tissue (Davidsson and Blennow, 1998; Canchi et al., 2019). The
283 consistent, age-independent dysregulation of this gene subset suggests that toxic tau
284 expression intrinsically alters the expression of key neuronal genes.

285 Notably, gene expression progressively changed with age in 10- and 20-day-old control flies
286 (Figure 2E). Importantly, the genes showing age-dependent expression changes in controls
287 exhibited exacerbated dysregulation in tauopathy flies, emerging as early as 2 days of age and
288 intensified markedly with age. These findings indicate that age-associated transcriptional shifts
289 are accelerated in a pathological tau-dependent manner, highlighting the aging cellular
290 environment as a key driver of tau-induced pathology and underscoring the profound impact of
291 age on disease-associated expression signatures.

292 Given the extensive neuronal cell death observed in 20-day-old tau transgenic flies, we focused
293 our subsequent transcriptomic analysis on 10-day-old flies to reduce the confounding effects of
294 neuronal cell loss on gene expression profiles (Figure 1B and Wittmann et al., 2001). At this age
295 time point, 17.4% of all expressed genes were differentially expressed in tau transgenic flies,
296 with 853 genes being downregulated and 787 genes upregulated (p-adj < 0.05, |FC| > 1.5)

297 (Figure 2B, Supplemental Data). We validated the RNA-seq findings using quantitative PCR
298 (qPCR) on independent replicates of 10-day-old control and tau transgenic flies, targeting 10
299 genes identified as significantly down- or up-regulated in the transcriptomic dataset (Figure
300 S2C, S2D).

301 Consistent with previous transcriptomic studies in tau transgenic models (Gjoneska et al., 2015;
302 Mangleburg et al., 2020), GO term analysis of downregulated genes revealed enrichment for
303 categories related to synaptic organization and neuronal function, including nervous system
304 processes, chemical synaptic transmission, and regulation of membrane potential (Figure 2F).
305 Among these, *hiw*, a gene encoding a RING E3 ubiquitin ligase playing an evolutionarily
306 conserved role in axonal development, was notably downregulated. Its human ortholog,
307 *MYCBP2,* has been linked to autism-like neurological symptoms when mutated (AlAbdi et al.,
308 2023). Another gene, *Ten-a*, was also downregulated in 10-day-old tau-expressing flies, and,
309 notably, a potential AD-related signal has been observed near the human TENM3 ortholog,
310 associated with amyloidosis and tau pathology in AD cohorts (Deming et al., 2018). Additionally,
311 *Gad1,* which encodes the enzyme responsible for synthesizing the inhibitory neurotransmitter
312 gamma-aminobutyric acid (GABA), was downregulated in our tauopathy model. This mirrors
313 the findings in chemically inactivated neurons, the aging human frontal cortex, and the
314 hippocampus of AD patients, suggesting that reduced neuronal inhibition is a shared feature of
315 aging and AD in both flies and humans (Blalock et al., 2004; Lu et al., 2004; Gleichmann et al.,
316 2012).

317 In 10-day-old tau transgenic flies, upregulated genes were significantly enriched for GO terms
318 associated with anabolic biological processes, such as small molecule biosynthesis and
319 cytoplasmic translation, as well as various catabolic pathways, including amino acid and
320 carbohydrate metabolism (Figure 2G). Notably, several cytochrome P450 genes - *Cyt-b5-r*,
321 *Cyp4d1*, *Cyp4e2*, *Cyp9b1*, and *Cyp6a17* - were upregulated, aligning with human studies that
322 report elevated levels of cytochrome P450 components in the cerebrospinal fluid and plasma in
323 antemortem AD patients over healthy controls (Borkowski et al., 2021). Additionally, genes
324 encoding proteins involved in immune response, particularly those from the immune deficiency
325 (imd) and Toll signaling pathways, were markedly upregulated in tau transgenic flies. This

326 robust activation of immune-related genes underscores chronic inflammation as a conserved
327 feature of tauopathy in both flies and humans (Langworth-Green et al., 2023).

328 An increased body of evidence suggests that tau contributes to neurodegeneration by
329 aberrantly reactivating the cell cycle in post-mitotic neurons, ultimately leading to apoptosis
330 (Khurana et al., 2006; Frost et al., 2014; Zhao et al., 2021a). Supporting this mechanism, our
331 transcriptomic analysis revealed upregulation of genes encoding proteins involved in DNA
332 replication and cell cycle progression, including proliferating cell nuclear antigen (*PCNA*), *Nnf1b*,
333 *Trithorax-like* (*Trl*), *Origin recognition complex subunit 1* (*Orc1*), and Minichromosome
334 maintenance 2 (*Mcm2*). We also observed increased expression of *Nucleophosmin* (*Nph*), a
335 gene that typically protects neurons but, when overexpressed, can promote cell cycle re-entry
336 and apoptosis (Pfister and D'Mello, 2015). Conversely, gene expression of Wee1 kinase (*Wee1*),
337 a key regulator of the G2/M checkpoint, was reduced, further supporting dysregulation of cell
338 cycle control (Esposito et al., 2021).

339 Collectively, these findings highlight the similarities between gene expression changes in the
340 *Drosophila* tauopathy model and those observed in human Alzheimer's disease. They also help
341 disentangle the distinct and overlapping contributions of aging and tau pathology to
342 transcriptomic alterations. Importantly, the gene expression changes identified in the 10-day-
343 old tau transgenic flies reveal early transcriptional disruptions associated with tau toxicity.
344 These include reduced synaptic signaling, increased immune response, and aberrant cell cycle
345 activation, all of which are key features of progressive tau-related neurodegeneration.

346

347 **<u>Figure 2 Legend</u>**

348 **(A)** Volcano plot showing differentially expressed genes (DEGs) between tau and control flies at
349 day 2, **(B)** day 10, and **(C)** day 20, post-eclosion. DEGs are identified using DESeq2 (adjusted p
350 value < 0.05, |FC| > 1.5). **(D)** Venn diagram illustrating the overlap between downregulated and
351 upregulated genes across all aging timepoints. **(E)** Heatmap showing trends in expression Z-
352 scores for all genes across all samples and aging timepoints. **(F)** Dot plot displaying the 20 most
353 significantly enriched biological process gene ontology (GO) terms for downregulated genes in

354 day 10 tau transgenics. **(G)** Dot plot illustrating the 15 most significantly enriched biological
355 process GO terms for upregulated genes in day 10 tau transgenics.

356 **Supplemental Figure 2 Legend**

357 **(A)** Principal component analysis (PCA) of longitudinal RNA-sequencing samples based on
358 normalized counts per million. **(B)** Hierarchically clustered heatmap of Pearson correlation
359 coefficients calculated from normalized RNA-seq expression values across all samples. Bar plots
360 displaying the relative transcript levels of genes assessed by qPCR that were identified as
361 downregulated **(C)** or upregulated **(D)** in tau transgenic flies by RNA sequencing. n=3-4
362 replicates of 20 male flies per genotype.

363

364 **3.3 Long genes with long introns are preferentially and significantly downregulated in tau**
365 **transgenic *Drosophila*.**

366 We previously demonstrated that long, highly expressed genes encoding proteins with
367 neuronal function tend to decrease expression in aging *Drosophila* photoreceptor neurons; a
368 decline that correlates with age-related visual impairment (Hall et al., 2017). Similar
369 associations between gene length, transcriptional output, and cellular function have been
370 reported across various tissues and organisms in both aging and neurodegenerative disease
371 contexts (Barbash and Sakmar, 2017; Lopes et al., 2021; Stoeger et al., 2022; Debès et al., 2023;
372 Gyenis et al., 2023). To explore whether similar features characterize genes dysregulated in our
373 tau transgenic flies, we analyzed transcriptomic data based on conserved genomic attributes
374 and expression levels. In 10-day-old tau transgenic flies, downregulated genes were
375 significantly longer than upregulated or unchanged genes (Figure 3A). Importantly, average
376 transcript abundance did not differ significantly between downregulated genes and other
377 differential expression groups (Figure S3A). GO term analysis of long downregulated genes
378 (>10kb) revealed enrichment for categories associated with neuronal structure and function,
379 including synapse organization and signaling (Figure 3B). Since neuronal genes are generally
380 longer than those expressed in other cell types (Zylka et al., 2015), we controlled for potential
381 bias by focusing on genes associated with GO0050877 (Nervous System Process), a highly

382 enriched and broadly encompassing neuronal GO term among downregulated genes (Figure
383 2C). Even within this subset, downregulated genes were significantly longer than genes in other
384 differential expression categories (Figure 3C). In contrast, long genes that did not change
385 expression in tau transgenic flies were associated with cell morphogenesis and developmental
386 processes (Figure 3D).

387 Gene length is shaped by both exon and intron architecture. While exons are short and highly
388 conserved, introns vary widely in length and can impact transcription efficiency (Carmel et al.,
389 2007; Yenerall and Zhou, 2012). In our tauopathy model, long genes that were significantly
390 downregulated contained more exons than genes with unchanged expression and
391 approximately twice as many as those in the upregulated gene group (Figure 3E). However, the
392 total length of their introns was four times that of genes with unchanged expression, averaging
393 approximately 22 kb, compared with approximately 5 kb for introns in genes with unchanged
394 expression (Figure 3F). Long intron splicing deficits in the tauopathy model may contribute to
395 gene dysregulation; however, at the transcript level, there is no change in the expression of key
396 splicing factors (Figure S3B). Overall, the observed difference in intron length largely explains
397 the increased total gene length observed in downregulated genes, suggesting that this genomic
398 feature may play a critical role in regulating proper gene expression in tauopathy flies.

399 **Figure 3 Legend**

400 **(A)** Violin and boxplot of differentially expressed gene (DEG) categories showing the total
401 length of all genes. **(B)** Dot plot displaying the 15 most enriched GO biological process terms
402 associated with long, downregulated genes. **(C)** Boxplot showing the length of genes within
403 'GO0050877: Nervous System Process' by DEG categories. **(D)** Dot plot displaying the 15 most
404 enriched GO biological process terms associated with long non-DEGs. Violin and boxplot of
405 differentially expressed gene (DEG) categories showing **(E)** number of exons, and **(F)** total intron
406 length. For differential expression data, DOWN (downregulated), NO (no change), and UP
407 (upregulated) expression in tau transgenic flies compared to controls at day 10 post-eclosion.
408 Long genes are defined as those > 10kb. ANOVA followed by TukeyHSD post-hoc test was used

409 to evaluate statistical significance between DEG groups (**** $p < 0.001$, * $p < 0.05$, NS/ns not
410 significant).

411 **Supplemental Figure 3 Legend**

412 **(A)** Violin and boxplot illustrating the expression of all long genes based on DEG categories.
413 Differential expression data are indicated as DOWN (downregulated), NO (no change), and UP
414 (upregulated) expression in tau transgenic flies compared to controls at day 10 post-eclosion.
415 Long genes are defined as > 10kb. ANOVA followed by TukeyHSD post-hoc test was used to
416 determine statistical significance between DEG groups (**** $p < 0.001$, *** $p < 0.005$, ** $p <$
417 0.01, *$p< 0.05$, NS/ns, not significant). **(B)** Dot plot displaying the 15 most enriched GO terms
418 among all non-DEGs.

419

420 **3.4 Increased promoter-proximal RNA polymerase II pausing is associated with long**
421 **downregulated genes.**

422 To focus our investigation of tau-dependent dysregulation of gene expression, we assessed
423 transcription dynamics using genome-wide profiling of RNAP II. After transcription initiation,
424 RNAP II typically pauses near the promoter, and its timely release into productive elongation is
425 a key regulatory step in fine-tuning gene expression. To map the RNAP II distribution in tau
426 transgenic flies, we assayed 10-day-old tau and age-matched control flies using the CUT&RUN
427 technique. This approach, combined with antibodies specific for Ser5- and Ser2-phosphorylated
428 (Ser5- and Ser2-P) RNAP II, markers of initiating and elongating forms of the polymerase,
429 respectively (Bozukova et al., 2022), enabled us to assess RNAP II dynamics with high
430 resolution.

431 CUT&RUN generated 3-6 million uniquely mapped fragments across four biological replicates
432 per genotype and antibody. Principal component analysis revealed that the primary source of
433 variance was RNAP II phosphorylation state (PC1) and tau expression (PC2) (Figure S4A). In
434 control flies, metaplot analysis revealed a sharp RNAP II peak around the TSS, followed by a
435 plateau across gene bodies and a decrease at the transcription end site (TES) (Figure 4A, first

436 column, gray line), consistent with a canonical RNAP II pattern across actively transcribed genes
437 (Bozukova et al., 2022). In contrast, tau transgenic flies showed elevated levels of initiating
438 RNAP II at the TSS and reduced levels of elongating RNAP II around the promoter and
439 throughout the gene body (Figure 4A, first column, yellow line). Stratifying RNAP II profiles by
440 gene expression revealed that both up- and downregulated genes in tau transgenic flies
441 exhibited increased initiating RNAP II occupancy at the TSS (Figure 4A, top row). For
442 upregulated genes, elongating RNAP II levels were comparable between tau-transgenic and
443 control flies, suggesting that increased transcript levels may result from enhanced transcription
444 initiation or increased RNA stability (Figure 4D, bottom row). Conversely, downregulated genes
445 exhibited a marked depletion of elongating RNAP II across gene bodies, consistent with reduced
446 transcriptional output.

447 To more specifically quantify pause proclivity in the tauopathy model, we calculated the RNAP II
448 Pause Index (PI), an initiation-to-elongation transition factor, for each gene. Building on
449 previously described RNAP II pause-release ratios (Akhtar et al., 2021), we integrated our
450 phospho-specific RNAP II dataset by defining the PI as the ratio of promoter-enriched Ser5-P
451 RNAP II to total gene body Ser2-P RNAP II occupancy for each gene in tauopathy versus control
452 flies (Figure 4B). Using this RNAP II PI as an unbiased, gene-level measurement of promoter-
453 proximal pausing, we uncovered a strong relationship between polymerase pausing, gene
454 expression changes, and gene length (Figure 4C, Figure S4B). Specifically, genes exhibiting
455 significantly increased promoter-proximal pausing were long and downregulated in tau-
456 transgenic flies. Further, within the most-paused gene cohort, those with the highest average
457 RNAP II PI, we identified several long, downregulated neuronal genes, including *Tomosyn* and
458 *Frq1*, that exemplify the canonical pattern of increased promoter proximal RNAP II pausing
459 (Figure 4D, E).

460 These findings reveal that RNAP II dynamics are specifically disrupted in the tauopathy model.
461 Notably, downregulated genes in tau transgenic flies are marked by the concomitant
462 accumulation of initiating RNAP II and depletion of elongating RNAP II. Taken together, these
463 RNAP II profiles suggest that exacerbated promoter-proximal polymerase pausing is a hallmark
464 of long, downregulated genes in the tauopathy model. This promoter-proximal polymerase

465 stalling may underlie failure of critical transcriptional processes, particularly the transition from
466 initiation to elongation, as a potential mechanism driving transcription stress in tauopathy.

467 **Figure 4 Legend:**

468 **(A)** Metaplots of CPM (counts per million)-normalized Ser2- and Ser5-phosphorylated RNAP II
469 CUT&RUN signals over gene bodies of all expressed protein-coding genes, all up- and
470 downregulated genes for control (gray) and tau transgenic flies (yellow). TSS, transcription start
471 site; TES, transcription end site. **(B)** Calculations for determining RNAP II Pause Index (PI). PI
472 values greater than 0 indicate increased promoter-proximal pausing for a given gene in the
473 tauopathy model. **(C)** Dot plot showing RNAP II pausing index (PI) values, gene expression, and
474 gene length. Genes were ranked by increasing PI score and grouped into 20 equal-sized bins.
475 Bin-wise means of PI value, gene expression, and gene length were plotted to visualize global
476 trends. **(D)** Genome browser inspection of RNAP II profiles in the Integrated Genomic Viewer
477 (IGV) depicting a representative long, downregulated neuronal gene, *Tomosyn*, from the
478 highest RNAP II PI bin. RNAP II density represents the average of four independent biological
479 replicates per genotype and RNAP II phosphor-isoform.

480

481 **Supplemental Figure 4 Legend:**

482 **(A)** PCA plot of RNAP II CUT&RUN samples based on consensus peak counts. The dot shape
483 indicates genotype, and the dot color indicates antibody target. **(B)** Dot plot showing the
484 correlation between RNAP II PI and gene expression for all expressed genes with an adjusted p-
485 value <0.05. Genome browser inspection of RNAP II profiles in the Integrated Genomic Viewer
486 (IGV) depicting representative long, downregulated neuronal genes, *Frq1* **(C)** and *nAChRalpha6*
487 **(D)**, from the highest RNAP II PI bin. RNAP II density represents the average of four independent
488 biological replicates per genotype and RNAP II phosphor-isoform.

489

490 **4. Discussion**

491 Gene dysregulation is a central hallmark of tauopathies, including Alzheimer's disease, and
492 underpins a range of pathological symptoms. Despite growing recognition of its importance,
493 our understanding of the multilayered regulation of gene expression, encompassing
494 transcriptional, epigenetic, and post-transcriptional mechanisms, in neurodegenerative disease
495 remains limited, particularly in the context of aging (Miller et al., 2008, 2010; Wan et al., 2020;
496 Tan et al., 2021). In this study, we used a well-established *Drosophila* tauopathy model with
497 neuronal expression of toxic human tau^{R406W}. Previously, the age-dependent transcriptome and
498 proteome of this tauopathy model were characterized in a comparative analysis to identify
499 intersectional trends in RNA and protein expression (Mangleburg et al., 2020). Here, we further
500 interrogated the ubiquitous and age-dependent transcriptional alterations driven by tau
501 accumulation and identified conserved genomic features of downregulated genes to elucidate
502 the underlying molecular mechanism driving gene dysregulation.

503 Tau-expressing flies exhibited preferential downregulation of genes required for maintaining
504 neuronal structure and function, including those involved in learning, memory, and locomotion.
505 Concurrently, we observed upregulation of genes associated with stress and immune
506 responses, metabolism, and cell cycle regulation. This tau-dependent gene-dysregulation
507 profile recapitulates age-related changes in expression. However, tau markedly accelerates and
508 amplifies age-dependent transcriptional stress, underscoring how aging and disease converge
509 to shape pathological gene expression signatures. These disrupted gene expression patterns
510 also mirror findings from other tau transgenic models, including aberrant cell cycle re-entry of
511 post-mitotic neurons, a process widely implicated as a key driver of neurodegeneration in
512 tauopathies and AD (Khurana et al., 2006; Zhao et al., 2021b).

513 Characterization of distinct genomic trends among differentially expressed genes in the
514 tauopathy model revealed that downregulated genes were significantly longer and had a four-
515 fold increase in cumulative intron length compared to non-differentially expressed genes. While
516 neuronal transcripts are generally longer than those of other cell types (Zylka et al., 2015), the
517 subset of downregulated neuronal genes in our dataset was notably longer than other neuron-

518 specific genes that were not differentially expressed. These findings align with a growing body
519 of research indicating an inverse relationship between gene length and transcriptional output in
520 the context of aging and neurodegenerative disease (Zylka et al., 2015; Hall et al., 2017; Gyenis
521 et al., 2023).

522 Further analysis revealed that long, downregulated genes in tau-expressing flies showed
523 reduced elongating RNAP II occupancy across gene bodies. These downregulated genes also
524 showed an accumulation of the initiating form of RNAP II just downstream of the transcription
525 start site, suggesting a failure to release promoter-proximal paused polymerase into active
526 elongation. On active genes, the transition of primed RNAP II into elongation is inhibited by
527 negative regulators NELF and DSIF, promoted by P-TEFb-mediated phosphorylation, and
528 maintained by other key histone modifiers and RNA-binding proteins (Jonkers and Lis, 2015). At
529 the transcript level, we observed no significant changes in the expression of these critical
530 elongation factors in the tauopathy fly model (data not shown). However, recent studies have
531 shown that transcription factors, splicing factors, and RNA-binding proteins can co-localize with
532 pathogenic tau tangles in the cytoplasm (Hsieh et al., 2019; Kavanagh et al., 2022), potentially
533 limiting their nuclear availability and regulatory function.

534 Notably, recent work in *Drosophila* shows that the nuclear exon junction core complex (pre-EJC)
535 associates with promoter regions through interactions with the initiating, Ser5-P RNAP II,
536 mediated by nascent RNA transcripts, thereby reinforcing promoter-proximal pausing. This
537 effect is particularly pronounced at genes containing long introns (Akhtar et al., 2019). In this
538 context, our findings further underscore, in particular, gene and intron length as critical
539 determinants of tau-induced transcriptional stress, suggesting that genes with these attributes
540 are especially susceptible to transcriptional dysregulation.

541 Gene dysregulation is a defining molecular hallmark of age-related diseases; yet, how these
542 regulatory pathways become disrupted in specific disease contexts remains a central question
543 in neurodegenerative disease biology. Our data reveal distinct transcriptional dynamics and
544 genomic features associated with downregulated transcripts in tauopathy, providing compelling
545 evidence that promoter-proximal RNAP II stalling is a hallmark of long neuronal genes. These

findings underscore the importance of studying gene regulatory mechanisms within disease-relevant contexts and highlight a pathological shift in transcriptional control in tauopathy. Future studies that elucidate the key factors in tau pathology that drive promoter-proximal RNAP II stalling and further clarify the connection between genomic features, such as gene and intron length, and RNAP II dynamics at vulnerable neuronal genes will help unravel the complexity of transcriptional regulation in age-related tauopathy. Furthermore, given the close interplay between genomic architecture, nascent RNA modifications, and chromatin structures in transcription regulation, investigating how these co-transcriptional elements collectively shape gene expression in neurodegeneration will be of significant interest.

Conflict Of Interest

The authors declare that the research was conducted in the absence of any commercial or financial relationships that could be construed as a potential conflict of interest.

Author Contributions

KC: Data curation, Formal Analysis, Investigation, Methodology, Visualization, Writing – original draft, review, and editing. NG: Formal analysis, Visualization, Writing–review. DF: Validation, Writing–review. GL: Validation, Writing–review. HH: Conceptualization, Funding acquisition, Resources, Supervision, Writing-review, and editing.

Funding

The authors declare that financial support was received from

Acknowledgments

Data Availability Statement

The RNA-seq and RNAP II CUT&RUN datasets generated for this study are available in the GEO repository [link].

575 **References**

576 Akhtar, J., Kreim, N., Marini, F., Mohana, G., Brüne, D., Binder, H., et al. (2019). Promoter-
577 proximal pausing mediated by the exon junction complex regulates splicing. *Nat*
578 *Commun* 10, 521. doi: 10.1038/s41467-019-08381-0

579 Akhtar, J., Renaud, Y., Albrecht, S., Ghavi-Helm, Y., Roignant, J.-Y., Silies, M., et al. (2021). m6A
580 RNA methylation regulates promoter- proximal pausing of RNA polymerase II. *Molecular*
581 *Cell* 81, 3356-3367.e6. doi: 10.1016/j.molcel.2021.06.023

582 AlAbdi, L., Desbois, M., Rusnac, D.-V., Sulaiman, R. A., Rosenfeld, J. A., Lalani, S., et al. (2023).
583 Loss-of-function variants in MYCBP2 cause neurobehavioural phenotypes and corpus
584 callosum defects. *Brain* 146, 1373–1387. doi: 10.1093/brain/awac364

585 Barbash, S., and Sakmar, T. P. (2017). Length-dependent gene misexpression is associated with
586 Alzheimer's disease progression. *Sci Rep* 7, 190. doi: 10.1038/s41598-017-00250-4

587 Black, M. M., Slaughter, T., Moshiach, S., Obrocka, M., and Fischer, I. (1996). Tau is enriched on
588 dynamic microtubules in the distal region of growing axons. *J Neurosci* 16, 3601–3619.
589 doi: 10.1523/JNEUROSCI.16-11-03601.1996

590 Blalock, E. M., Geddes, J. W., Chen, K. C., Porter, N. M., Markesbery, W. R., and Landfield, P. W.
591 (2004). Incipient Alzheimer's disease: Microarray correlation analyses reveal major
592 transcriptional and tumor suppressor responses. *Proceedings of the National Academy*
593 *of Sciences* 101, 2173–2178. doi: 10.1073/pnas.0308512100

594 Bolger, A. M., Lohse, M., and Usadel, B. (2014). Trimmomatic: a flexible trimmer for Illumina
595 sequence data. *Bioinformatics* 30, 2114–2120. doi: 10.1093/bioinformatics/btu170

596 Borkowski, K., Pedersen, T. L., Seyfried, N. T., Lah, J. J., Levey, A. I., Hales, C. M., et al. (2021).
597 Association of plasma and CSF cytochrome P450, soluble epoxide hydrolase, and
598 ethanolamide metabolism with Alzheimer's disease. *Alzheimers Res Ther* 13, 149. doi:
599 10.1186/s13195-021-00893-6

600 Bozukova, M., Nikopoulou, C., Kleinenkuhnen, N., Grbavac, D., Goetsch, K., and Tessarz, P.
601 (2022). Aging is associated with increased chromatin accessibility and reduced
602 polymerase pausing in liver. *Molecular Systems Biology* 18, e11002. doi:
603 10.15252/msb.202211002

604 Bustin, S. A., Benes, V., Garson, J. A., Hellemans, J., Huggett, J., Kubista, M., et al. (2009). The
605 MIQE Guidelines: Minimum Information for Publication of Quantitative Real-Time PCR
606 Experiments. *Clinical Chemistry* 55, 611–622. doi: 10.1373/clinchem.2008.112797

607 Canchi, S., Raao, B., Masliah, D., Rosenthal, S. B., Sasik, R., Fisch, K. M., et al. (2019). Integrating
608 Gene and Protein Expression Reveals Perturbed Functional Networks in Alzheimer's
609 Disease. *Cell Rep* 28, 1103-1116.e4. doi: 10.1016/j.celrep.2019.06.073

610 Carmel, L., Rogozin, I. B., Wolf, Y. I., and Koonin, E. V. (2007). Patterns of intron gain and
611 conservation in eukaryotic genes. *BMC evolutionary biology* 7, 192. doi: 10.1186/1471-
612 2148-7-192

613 Chen, S., Zhou, Y., Chen, Y., and Gu, J. (2018). fastp: an ultra-fast all-in-one FASTQ preprocessor.
614 *Bioinformatics* 34, i884–i890. doi: 10.1093/bioinformatics/bty560

615 Creekmore, B. C., Watanabe, R., and Lee, E. B. (2024). Neurodegenerative Disease Tauopathies.
616 *Annu Rev Pathol* 19, 345–370. doi: 10.1146/annurev-pathmechdis-051222-120750

617 Davidsson, P., and Blennow, K. (1998). Neurochemical dissection of synaptic pathology in
618 Alzheimer's disease. *Int Psychogeriatr* 10, 11–23. doi: 10.1017/s1041610298005110

619 Debès, C., Papadakis, A., Grönke, S., Karalay, Ö., Tain, L. S., Mizi, A., et al. (2023). Ageing-
620 associated changes in transcriptional elongation influence longevity. *Nature* 616, 814–
621 821. doi: 10.1038/s41586-023-05922-y

622 Deming, Y., Dumitrescu, L., Barnes, L. L., Thambisetty, M., Kunkle, B., Gifford, K. A., et al. (2018).
623 Sex-specific genetic predictors of Alzheimer's disease biomarkers. *Acta Neuropathol*
624 136, 857–872. doi: 10.1007/s00401-018-1881-4

625 Esposito, F., Giuffrida, R., Raciti, G., Puglisi, C., and Forte, S. (2021). Wee1 Kinase: A Potential
626 Target to Overcome Tumor Resistance to Therapy. *Int J Mol Sci* 22, 10689. doi:
627 10.3390/ijms221910689

628 Frost, B., Hemberg, M., Lewis, J., and Feany, M. B. (2014). Tau promotes neurodegeneration
629 through global chromatin relaxation. *Nat Neurosci* 17, 357–366. doi: 10.1038/nn.3639

630 Gjoneska, E., Pfenning, A. R., Mathys, H., Quon, G., Kundaje, A., Tsai, L.-H., et al. (2015).
631 Conserved epigenomic signals in mice and humans reveal immune basis of Alzheimer's
632 disease. *Nature* 518, 365–369. doi: 10.1038/nature14252

633 Gleichmann, M., Zhang, Y., Wood, W. H., Becker, K. G., Mughal, M. R., Pazin, M. J., et al. (2012).
634 Molecular changes in brain aging and Alzheimer's disease are mirrored in
635 experimentally silenced cortical neuron networks. *Neurobiol Aging* 33, 205.e1-205.e18.
636 doi: 10.1016/j.neurobiolaging.2010.08.012

637 Goedert, M., and Spillantini, M. G. (2000). Tau mutations in frontotemporal dementia FTDP-17
638 and their relevance for Alzheimer's disease. *Biochim Biophys Acta* 1502, 110–121. doi:
639 10.1016/s0925-4439(00)00037-5

640 Gyenis, A., Chang, J., Demmers, J. J. P. G., Bruens, S. T., Barnhoorn, S., Brandt, R. M. C., et al.
641 (2023). Genome-wide RNA polymerase stalling shapes the transcriptome during aging.
642 *Nat Genet* 55, 268–279. doi: 10.1038/s41588-022-01279-6

643 Hall, H., Medina, P., Cooper, D. A., Escobedo, S. E., Rounds, J., Brennan, K. J., et al. (2017).
644 Transcriptome profiling of aging Drosophila photoreceptors reveals gene expression
645 trends that correlate with visual senescence. *BMC Genomics* 18, 894. doi:
646 10.1186/s12864-017-4304-3

647 Hong, M., Zhukareva, V., Vogelsberg-Ragaglia, V., Wszolek, Z., Reed, L., Miller, B. I., et al. (1998).
648 Mutation-specific functional impairments in distinct tau isoforms of hereditary FTDP-17.
649 *Science* 282, 1914–1917. doi: 10.1126/science.282.5395.1914

650 Hsieh, Y.-C., Guo, C., Yalamanchili, H. K., Abreha, M., Al-Ouran, R., Li, Y., et al. (2019). Tau-
651 Mediated Disruption of the Spliceosome Triggers Cryptic RNA Splicing and
652 Neurodegeneration in Alzheimer's Disease. *Cell Rep* 29, 301-316.e10. doi:
653 10.1016/j.celrep.2019.08.104

654 Hutton, M. (2000). Molecular Genetics of Chromosome 17 Tauopathies. *Annals of the New York*
655 *Academy of Sciences* 920, 63–73. doi: 10.1111/j.1749-6632.2000.tb06906.x

656 Ikeda, M., Shoji†, M., Kawarai, T., Kawarabayashi, T., Matsubara, E., Murakami, T., et al. (2005).
657 Accumulation of Filamentous Tau in the Cerebral Cortex of Human Tau R406W
658 Transgenic Mice. *Am J Pathol* 166, 521–531.

659 Jauregui-Lozano, J., Escobedo, S., Easton, A., Lanman, N. A., Weake, V. M., and Hall, H. (2022).
660 Proper control of R-loop homeostasis is required for maintenance of gene expression
661 and neuronal function during aging. *Aging Cell* 21, e13554. doi: 10.1111/acel.13554

662 Jonkers, I., and Lis, J. T. (2015). Getting up to speed with transcription elongation by RNA
663 polymerase II. *Nat Rev Mol Cell Biol* 16, 167–177. doi: 10.1038/nrm3953

664 Kavanagh, T., Halder, A., and Drummond, E. (2022). Tau interactome and RNA binding proteins
665 in neurodegenerative diseases. *Molecular Neurodegeneration* 17, 66. doi:
666 10.1186/s13024-022-00572-6

667 Khurana, V., Lu, Y., Steinhilb, M. L., Oldham, S., Shulman, J. M., and Feany, M. B. (2006). TOR-
668 Mediated Cell-Cycle Activation Causes Neurodegeneration in a *Drosophila* Tauopathy
669 Model. *Current Biology* 16, 230–241. doi: 10.1016/j.cub.2005.12.042

670 Kim, J., Selvaraji, S., Kang, S. W., Lee, W. T., Chen, C. L.-H., Choi, H., et al. (2019). Cerebral
671 transcriptome analysis reveals age-dependent progression of neuroinflammation in
672 P301S mutant tau transgenic male mice. *Brain Behav Immun* 80, 344–357. doi:
673 10.1016/j.bbi.2019.04.011

674 Krishnamurthy, P. K., and Johnson, G. V. W. (2004). Mutant (R406W) Human Tau Is
675 Hyperphosphorylated and Does Not Efficiently Bind Microtubules in a Neuronal Cortical
676 Cell Model*. *Journal of Biological Chemistry* 279, 7893–7900. doi:
677 10.1074/jbc.M311203200

678 Langmead, B., and Salzberg, S. L. (2012). Fast gapped-read alignment with Bowtie 2. *Nat*
679 *Methods* 9, 357–359. doi: 10.1038/nmeth.1923

680 Langworth-Green, C., Patel, S., Jaunmuktane, Z., Jabbari, E., Morris, H., Thom, M., et al. (2023).
681 Chronic effects of inflammation on tauopathies. *Lancet Neurol* 22, 430–442. doi:
682 10.1016/S1474-4422(23)00038-8

683 Lopes, I., Altab, G., Raina, P., and de Magalhães, J. P. (2021). Gene Size Matters: An Analysis of
684 Gene Length in the Human Genome. *Front. Genet.* 12. doi: 10.3389/fgene.2021.559998

685 López-Otín, C., Blasco, M. A., Partridge, L., Serrano, M., and Kroemer, G. (2023). Hallmarks of
686 aging: An expanding universe. *Cell* 186, 243–278. doi: 10.1016/j.cell.2022.11.001

687 Love, M. I., Huber, W., and Anders, S. (2014). Moderated estimation of fold change and
688 dispersion for RNA-seq data with DESeq2. *Genome Biology* 15, 550. doi:
689 10.1186/s13059-014-0550-8

690 Lu, T., Pan, Y., Kao, S.-Y., Li, C., Kohane, I., Chan, J., et al. (2004). Gene regulation and DNA
691 damage in the ageing human brain. *Nature* 429, 883–891. doi: 10.1038/nature02661

692 Mangleburg, C. G., Wu, T., Yalamanchili, H. K., Guo, C., Hsieh, Y.-C., Duong, D. M., et al. (2020).
693 Integrated analysis of the aging brain transcriptome and proteome in tauopathy.
694 *Molecular Neurodegeneration* 15, 56. doi: 10.1186/s13024-020-00405-4

695 Merlo, P., Frost, B., Peng, S., Yang, Y. J., Park, P. J., and Feany, M. (2014). p53 prevents
696 neurodegeneration by regulating synaptic genes. *Proceedings of the National Academy*
697 *of Sciences* 111, 18055–18060. doi: 10.1073/pnas.1419083111

698 Miller, J. A., Horvath, S., and Geschwind, D. H. (2010). Divergence of human and mouse brain
699 transcriptome highlights Alzheimer disease pathways. *Proceedings of the National*
700 *Academy of Sciences* 107, 12698–12703. doi: 10.1073/pnas.0914257107

701 Miller, J. A., Oldham, M. C., and Geschwind, D. H. (2008). A Systems Level Analysis of
702 Transcriptional Changes in Alzheimer's Disease and Normal Aging. *J Neurosci* 28, 1410–
703 1420. doi: 10.1523/JNEUROSCI.4098-07.2008

704 Mostafavi, S., Gaiteri, C., Sullivan, S. E., White, C. C., Tasaki, S., Xu, J., et al. (2018). A molecular
705 network of the aging human brain provides insights into the pathology and cognitive
706 decline of Alzheimer's disease. *Nat Neurosci* 21, 811–819. doi: 10.1038/s41593-018-
707 0154-9

708 Nakamura, M., Shiozawa, S., Tsuboi, D., Amano, M., Watanabe, H., Maeda, S., et al. (2019).
709 Pathological Progression Induced by the Frontotemporal Dementia-Associated R406W
710 Tau Mutation in Patient-Derived iPSCs. *Stem Cell Reports* 13, 684–699. doi:
711 10.1016/j.stemcr.2019.08.011

712 Niccoli, T., and Partridge, L. (2012). Ageing as a Risk Factor for Disease. *Current Biology* 22,
713 R741–R752. doi: 10.1016/j.cub.2012.07.024

714 Nyakas, C., Granic, I., Halmy, L. G., Banerjee, P., and Luiten, P. G. M. (2011). The basal forebrain
715 cholinergic system in aging and dementia. Rescuing cholinergic neurons from neurotoxic
716 amyloid-β42 with memantine. *Behavioural Brain Research* 221, 594–603. doi:
717 10.1016/j.bbr.2010.05.033

718 Patro, R., Duggal, G., Love, M. I., Irizarry, R. A., and Kingsford, C. (2017). Salmon: fast and bias-
719 aware quantification of transcript expression using dual-phase inference. *Nat Methods*
720 14, 417–419. doi: 10.1038/nmeth.4197

721 Pfister, J. A., and D'Mello, S. R. (2015). Insights into the regulation of neuronal viability by
722 nucleophosmin/B23. *Experimental Biology and Medicine* 240, 774. doi:
723 10.1177/1535370215579168

724 Quinlan, A. R., and Hall, I. M. (2010). BEDTools: a flexible suite of utilities for comparing
725 genomic features. *Bioinformatics* 26, 841–842. doi: 10.1093/bioinformatics/btq033

726 Ramírez, G., Alvarez, A., Garcia-Abreu, J., Gomes, F. C., Moura Neto, V., and Maccioni, R. B.
727 (1999). Regulatory roles of microtubule-associated proteins in neuronal morphogenesis.
728 Involvement of the extracellular matrix. *Braz J Med Biol Res* 32, 611–618. doi:
729 10.1590/s0100-879x1999000500015

730 Stegeman, R., Hall, H., Escobedo, S. E., Chang, H. C., and Weake, V. M. (2018). Proper splicing
731 contributes to visual function in the aging Drosophila eye. *Aging Cell* 17, e12817. doi:
732 10.1111/acel.12817

733 Stoeger, T., Grant, R. A., McQuattie-Pimentel, A. C., Anekalla, K. R., Liu, S. S., Tejedor-Navarro,
734 H., et al. (2022). Aging is associated with a systemic length-associated transcriptome
735 imbalance. *Nat Aging* 2, 1191–1206. doi: 10.1038/s43587-022-00317-6

736 Tan, M.-S., Yang, Y.-X., Xu, W., Wang, H.-F., Tan, L., Zuo, C.-T., et al. (2021). Associations of
737 Alzheimer's disease risk variants with gene expression, amyloidosis, tauopathy, and
738 neurodegeneration. *Alzheimer's Research & Therapy* 13, 15. doi: 10.1186/s13195-020-
739 00755-7

740 Tatebayashi, Y., Miyasaka, T., Chui, D.-H., Akagi, T., Mishima, K., Iwasaki, K., et al. (2002). Tau
741 filament formation and associative memory deficit in aged mice expressing mutant
742 (R406W) human tau. *Proc Natl Acad Sci U S A* 99, 13896–13901. doi:
743 10.1073/pnas.202205599

744 Wan, Y.-W., Al-Ouran, R., Mangleburg, C. G., Perumal, T. M., Lee, T. V., Allison, K., et al. (2020).
745 Meta-Analysis of the Alzheimer's Disease Human Brain Transcriptome and Functional
746 Dissection in Mouse Models. *Cell Reports* 32, 107908. doi: 10.1016/j.celrep.2020.107908

747 Wittmann, C. W., Wszolek, M. F., Shulman, J. M., Salvaterra, P. M., Lewis, J., Hutton, M., et al.
748 (2001). Tauopathy in Drosophila: Neurodegeneration Without Neurofibrillary Tangles.
749 *Science* 293, 711–714. doi: 10.1126/science.1062382

750 Wszolek, Z. K., Tsuboi, Y., Ghetti, B., Pickering-Brown, S., Baba, Y., and Cheshire, W. P. (2006).
751 Frontotemporal dementia and parkinsonism linked to chromosome 17 (FTDP-17).
752 *Orphanet J Rare Dis* 1, 30. doi: 10.1186/1750-1172-1-30

753 Yenerall, P., and Zhou, L. (2012). Identifying the mechanisms of intron gain: progress and
754 trends. *Biology Direct* 7, 29. doi: 10.1186/1745-6150-7-29

755 Yu, G., Wang, L.-G., Han, Y., and He, Q.-Y. (2012). clusterProfiler: an R Package for Comparing
756 Biological Themes Among Gene Clusters. *OMICS* 16, 284–287. doi:
757 10.1089/omi.2011.0118

758 Zhang, B., Higuchi, M., Yoshiyama, Y., Ishihara, T., Forman, M. S., Martinez, D., et al. (2004).
759 Retarded axonal transport of R406W mutant tau in transgenic mice with a
760 neurodegenerative tauopathy. *J Neurosci* 24, 4657–4667. doi:
761 10.1523/JNEUROSCI.0797-04.2004

762 Zhang, Y., Liu, T., Meyer, C. A., Eeckhoute, J., Johnson, D. S., Bernstein, B. E., et al. (2008).
763 Model-based Analysis of ChIP-Seq (MACS). *Genome Biology* 9, R137. doi: 10.1186/gb-
764 2008-9-9-r137

765 Zhao, F., Xu, Y., Gao, S., Qin, L., Austria, Q., Siedlak, S. L., et al. (2021a). METTL3-dependent RNA
766 m6A dysregulation contributes to neurodegeneration in Alzheimer's disease through
767 aberrant cell cycle events. *Mol Neurodegener* 16, 70. doi: 10.1186/s13024-021-00484-x

768 Zhao, F., Xu, Y., Gao, S., Qin, L., Austria, Q., Siedlak, S. L., et al. (2021b). METTL3-dependent RNA
769 m6A dysregulation contributes to neurodegeneration in Alzheimer's disease through
770 aberrant cell cycle events. *Mol Neurodegener* 16, 70. doi: 10.1186/s13024-021-00484-x

771 Zylka, M. J., Simon, J. M., and Philpot, B. D. (2015). Gene Length Matters in Neurons. *Neuron* 86,
772 353–355. doi: 10.1016/j.neuron.2015.03.059

773

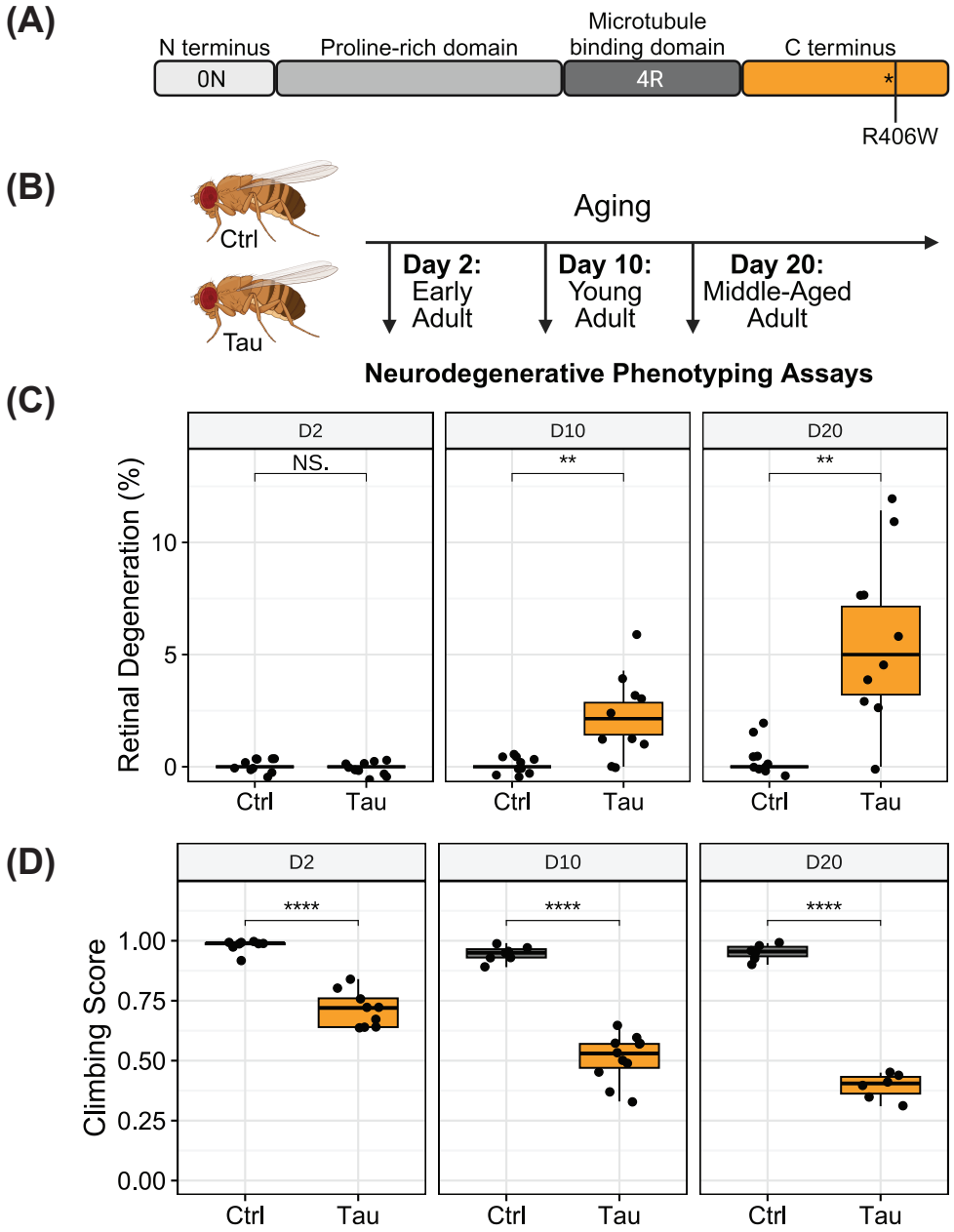
(A)
N terminus
Proline-rich domain
Microtubule binding domain
C terminus
0N
4R
*
R406W
(B)
Ctrl
Tau
Aging
Day 2: Early Adult
Day 10: Young Adult
Day 20: Middle-Aged Adult
Neurodegenerative Phenotyping Assays
(C)
D2
D10
D20
NS.
**
**
Retinal Degeneration (%)
0
5
10
Ctrl
Tau
(D)
D2
D10
D20
****
****
****
Climbing Score
0.00
0.25
0.50
0.75
1.00
Ctrl
Tau

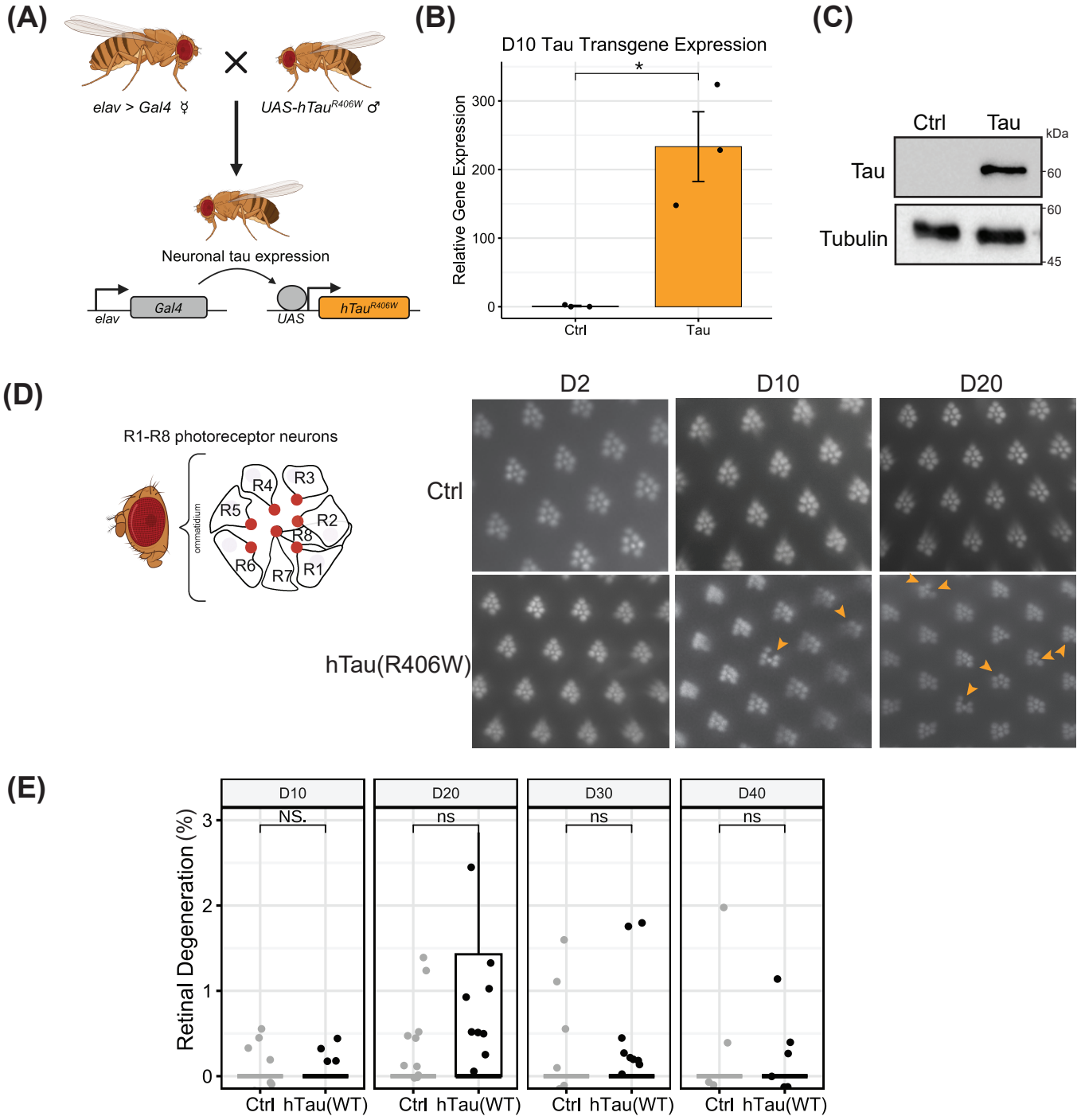
(A)
elav > Gal4 ♀
UAS-hTau^{R406W} ♂
Neuronal tau expression
elav
Gal4
UAS
hTau^{R406W}
(B)
D10 Tau Transgene Expression
Relative Gene Expression
300
200
100
0
*
Ctrl
Tau
(C)
Ctrl
Tau
kDa
Tau
60
Tubulin
60
45
(D)
R1-R8 photoreceptor neurons
ommatidium
R1
R2
R3
R4
R5
R6
R7
R8
D2
D10
D20
Ctrl
hTau(R406W)
(E)
D10
D20
D30
D40
NS.
ns
ns
ns
Retinal Degeneration (%)
3
2
1
0
Ctrl
hTau(WT)
Ctrl
hTau(WT)
Ctrl
hTau(WT)
Ctrl
hTau(WT)

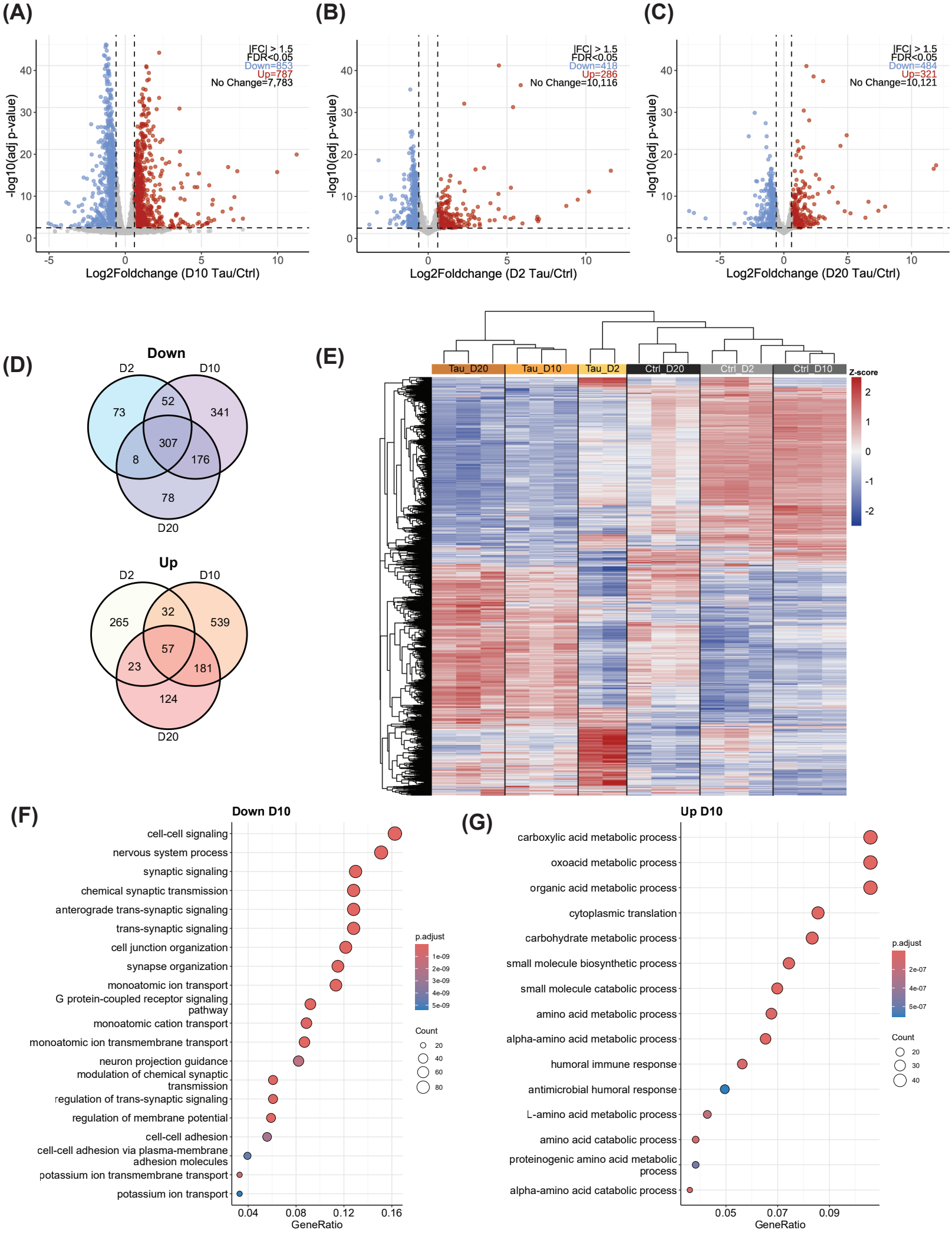
(A)
|FC| > 1.5
FDR<0.05
Down=853
Up=787
No Change=7,783
-log10(adj p-value)
Log2Foldchange (D10 Tau/Ctrl)
(B)
|FC| > 1.5
FDR<0.05
Down=418
Up=286
No Change=10,116
-log10(adj p-value)
Log2Foldchange (D2 Tau/Ctrl)
(C)
|FC| > 1.5
FDR<0.05
Down=484
Up=321
No Change=10,121
-log10(adj p-value)
Log2Foldchange (D20 Tau/Ctrl)
(D)
Down
D2
D10
D20
73
52
341
307
8
176
78
Up
D2
D10
D20
265
32
539
57
23
181
124
(E)
Tau_D20
Tau_D10
Tau_D2
Ctrl_D20
Ctrl_D2
Ctrl_D10
Z-score
2
1
0
-1
-2
(F)
Down D10
cell-cell signaling
nervous system process
synaptic signaling
chemical synaptic transmission
anterograde trans-synaptic signaling
trans-synaptic signaling
cell junction organization
synapse organization
monoatomic ion transport
G protein-coupled receptor signaling pathway
monoatomic cation transport
monoatomic ion transmembrane transport
neuron projection guidance
modulation of chemical synaptic transmission
regulation of trans-synaptic signaling
regulation of membrane potential
cell-cell adhesion
cell-cell adhesion via plasma-membrane adhesion molecules
potassium ion transmembrane transport
potassium ion transport
0.04
0.08
0.12
0.16
GeneRatio
p.adjust
1e-09
2e-09
3e-09
4e-09
5e-09
Count
20
40
60
80
(G)
Up D10
carboxylic acid metabolic process
oxoacid metabolic process
organic acid metabolic process
cytoplasmic translation
carbohydrate metabolic process
small molecule biosynthetic process
small molecule catabolic process
amino acid metabolic process
alpha-amino acid metabolic process
humoral immune response
antimicrobial humoral response
L-amino acid metabolic process
amino acid catabolic process
proteinogenic amino acid metabolic process
alpha-amino acid catabolic process
0.05
0.07
0.09
GeneRatio
p.adjust
2e-07
4e-07
6e-07
Count
20
30
40

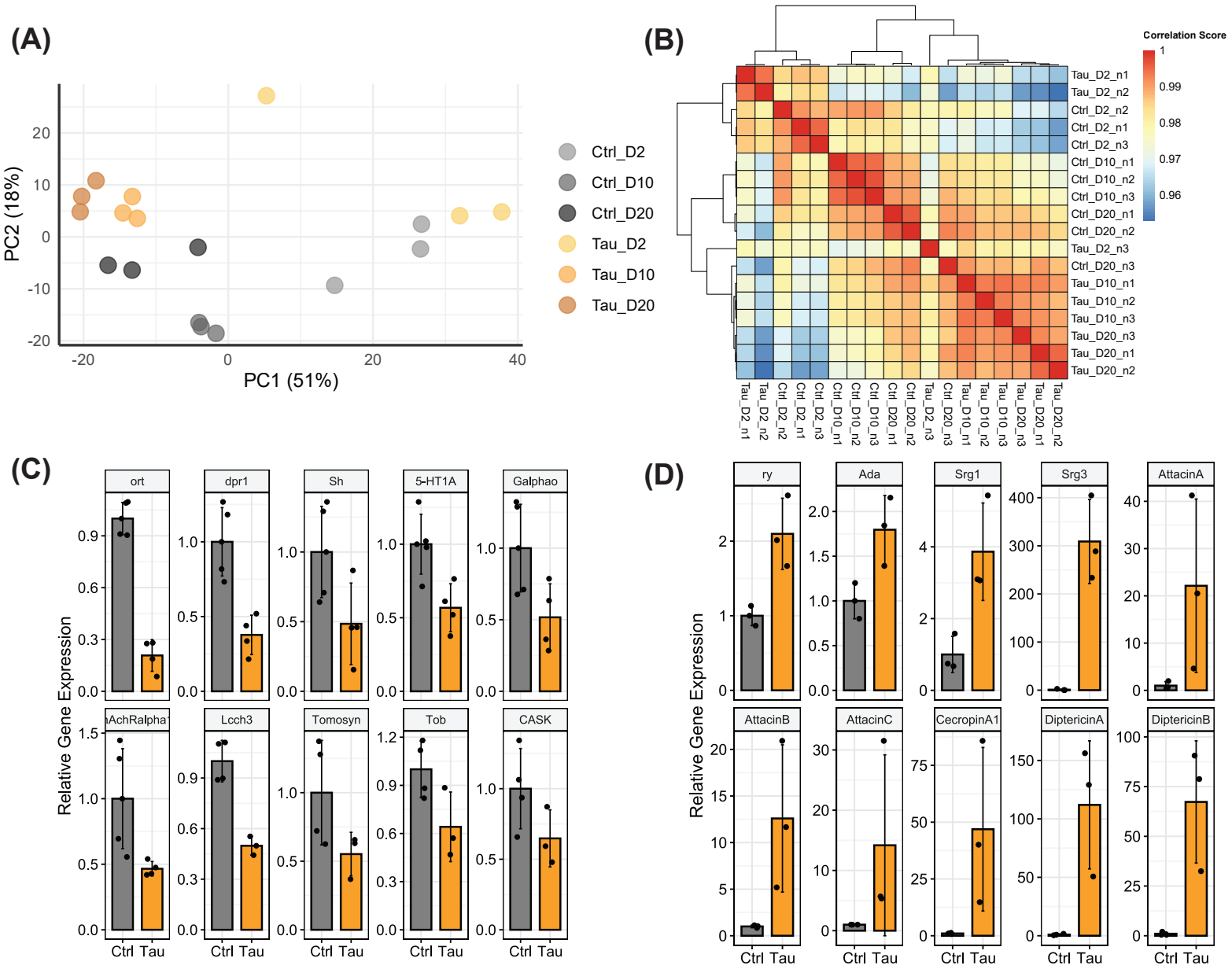
(A)
PC2 (18%)
PC1 (51%)
Ctrl_D2
Ctrl_D10
Ctrl_D20
Tau_D2
Tau_D10
Tau_D20
(B)
Correlation Score
Tau_D2_n1
Tau_D2_n2
Ctrl_D2_n2
Ctrl_D2_n1
Ctrl_D2_n3
Ctrl_D10_n1
Ctrl_D10_n2
Ctrl_D10_n3
Ctrl_D20_n1
Ctrl_D20_n2
Tau_D2_n3
Ctrl_D20_n3
Tau_D10_n1
Tau_D10_n2
Tau_D10_n3
Tau_D20_n3
Tau_D20_n1
Tau_D20_n2
(C)
ort
dpr1
Sh
5-HT1A
Galphao
AChRalpha7
Lcch3
Tomosyn
Tob
CASK
Relative Gene Expression
Ctrl Tau
(D)
ry
Ada
Srg1
Srg3
AttacinA
AttacinB
AttacinC
CecropinA1
DiptericinA
DiptericinB
Relative Gene Expression
Ctrl Tau

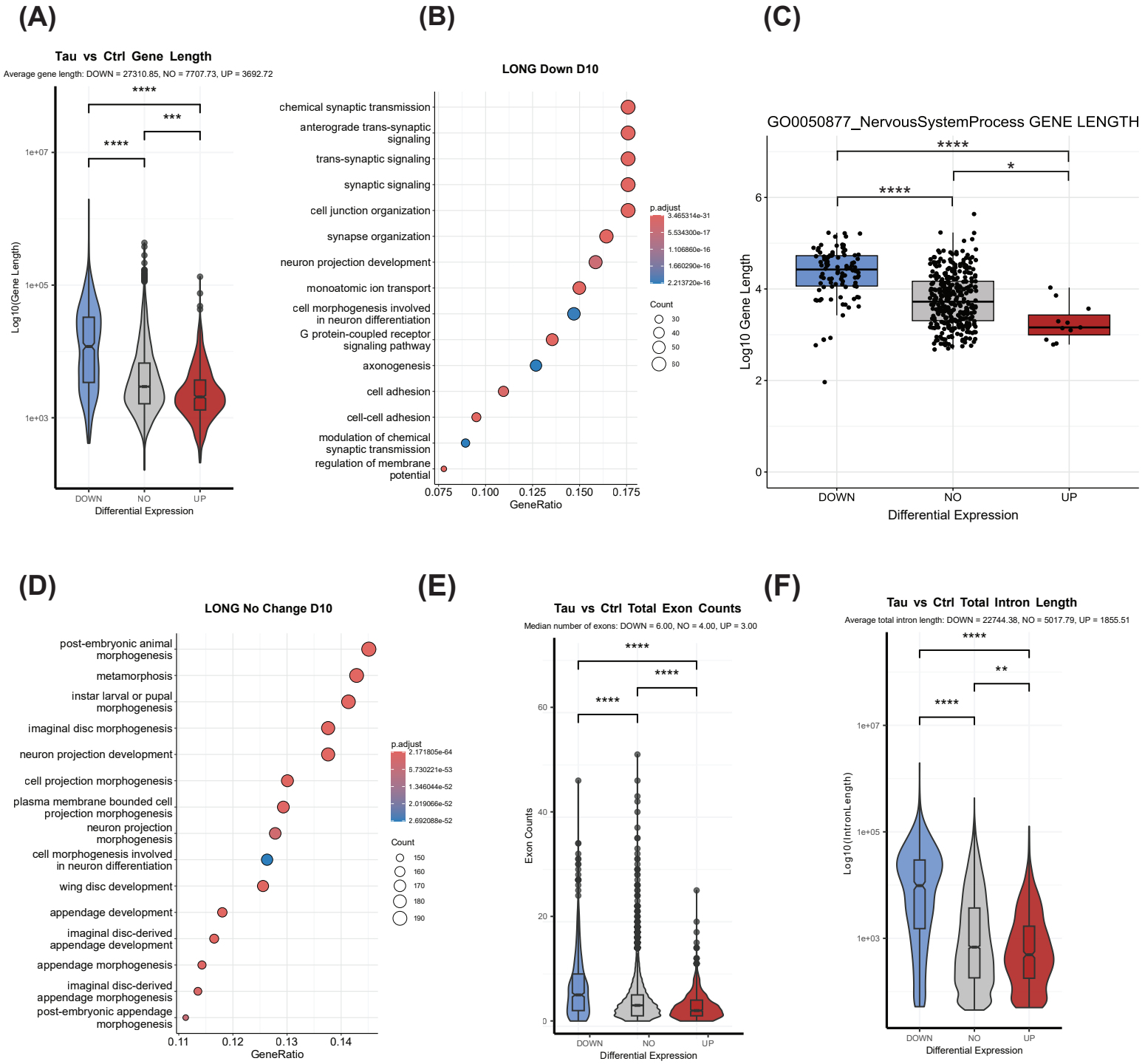
(A)
Tau vs Ctrl Gene Length
Average gene length: DOWN = 27310.85, NO = 7707.73, UP = 3692.72
****
***
****
1e+07
1e+05
1e+03
Log10(Gene Length)
DOWN
NO
UP
Differential Expression
(B)
LONG Down D10
chemical synaptic transmission
anterograde trans-synaptic signaling
trans-synaptic signaling
synaptic signaling
cell junction organization
synapse organization
neuron projection development
monoatomic ion transport
cell morphogenesis involved in neuron differentiation
G protein-coupled receptor signaling pathway
axonogenesis
cell adhesion
cell-cell adhesion
modulation of chemical synaptic transmission
regulation of membrane potential
0.075
0.100
0.125
0.150
0.175
GeneRatio
p.adjust
3.465314e-31
5.534300e-17
1.106860e-16
1.660290e-16
2.213720e-16
Count
30
40
50
60
(C)
GO0050877_NervousSystemProcess GENE LENGTH
****
*
****
6
4
2
0
Log10 Gene Length
DOWN
NO
UP
Differential Expression
(D)
LONG No Change D10
post-embryonic animal morphogenesis
metamorphosis
instar larval or pupal morphogenesis
imaginal disc morphogenesis
neuron projection development
cell projection morphogenesis
plasma membrane bounded cell projection morphogenesis
neuron projection morphogenesis
cell morphogenesis involved in neuron differentiation
wing disc development
appendage development
imaginal disc-derived appendage development
appendage morphogenesis
imaginal disc-derived appendage morphogenesis
post-embryonic appendage morphogenesis
0.11
0.12
0.13
0.14
GeneRatio
p.adjust
2.171805e-64
5.730221e-53
1.346044e-52
2.019066e-52
2.692088e-52
Count
150
160
170
180
190
(E)
Tau vs Ctrl Total Exon Counts
Median number of exons: DOWN = 6.00, NO = 4.00, UP = 3.00
****
****
****
60
40
20
0
Exon Counts
DOWN
NO
UP
Differential Expression
(F)
Tau vs Ctrl Total Intron Length
Average total intron length: DOWN = 22744.38, NO = 5017.79, UP = 1855.51
****
**
****
1e+07
1e+05
1e+03
Log10(IntronLength)
DOWN
NO
UP
Differential Expression

(A)

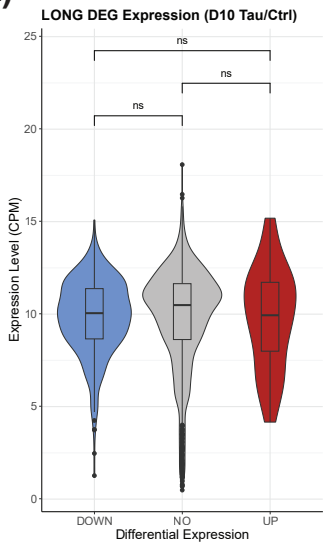
LONG DEG Expression (D10 Tau/Ctrl)
ns
ns
ns
Expression Level (CPM)
25
20
15
10
5
0
DOWN
NO
UP
Differential Expression

(B)

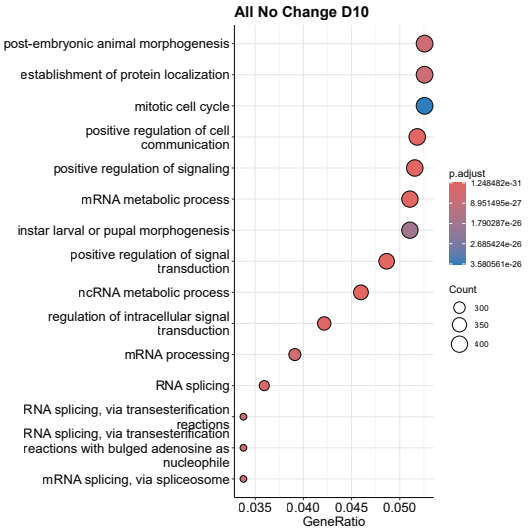
All No Change D10
post-embryonic animal morphogenesis
establishment of protein localization
mitotic cell cycle
positive regulation of cell communication
positive regulation of signaling
mRNA metabolic process
instar larval or pupal morphogenesis
positive regulation of signal transduction
ncRNA metabolic process
regulation of intracellular signal transduction
mRNA processing
RNA splicing
RNA splicing, via transesterification reactions
RNA splicing, via transesterification reactions with bulged adenosine as nucleophile
mRNA splicing, via spliceosome
0.035
0.040
0.045
0.050
GeneRatio
p.adjust
1.248482e-31
8.951495e-27
1.790287e-26
2.685424e-26
3.580561e-26
Count
300
350
400

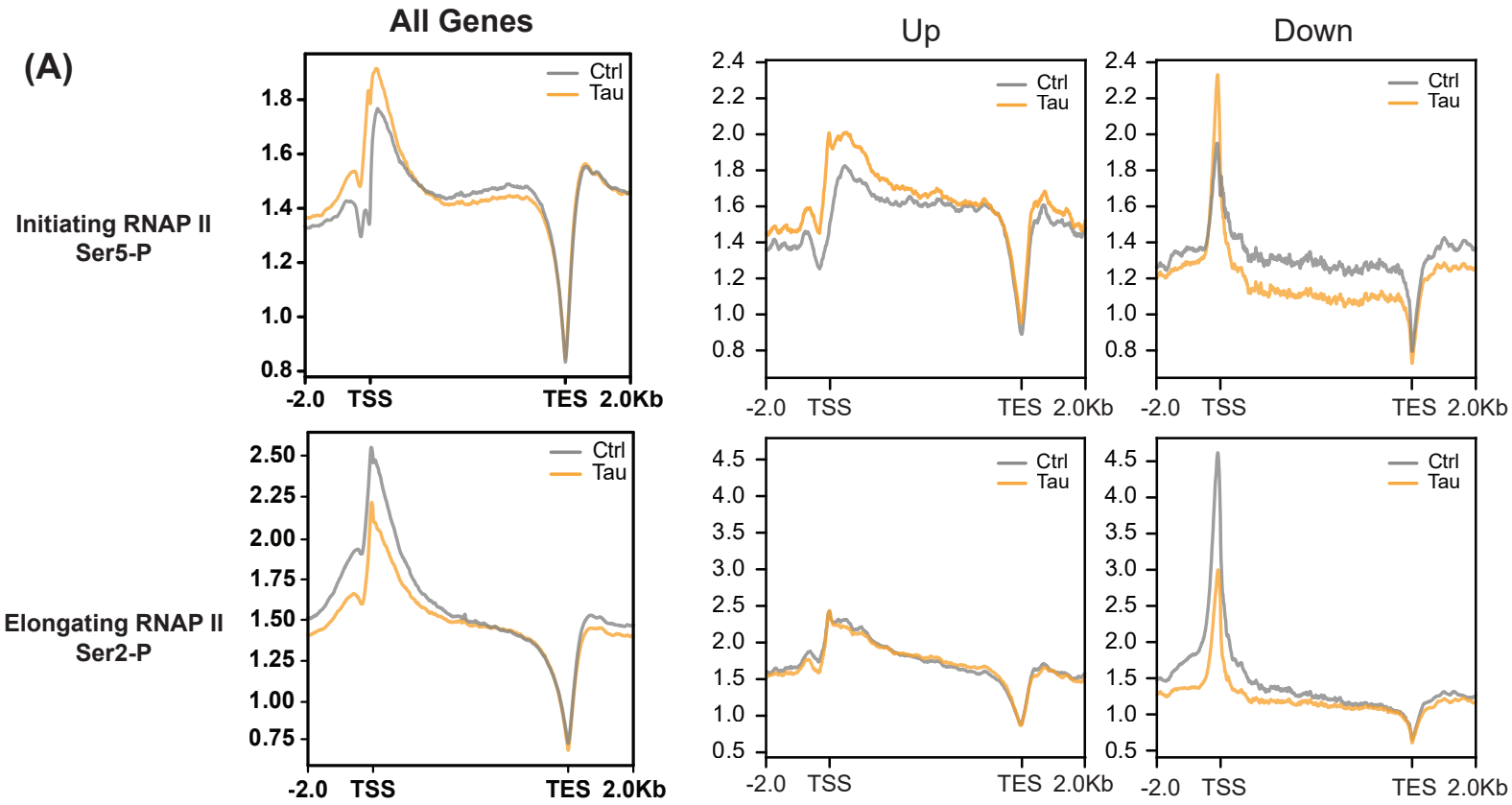

(B)

$$\log\left(\frac{\left(\frac{Ser5P\ Promoter}{Ser5P\ Gene\ Body}\right)^{Tau}}{\left(\frac{Ser5P\ Promoter}{Ser5P\ Gene\ Body}\right)^{Ctrl}}\right) - \log\left(\frac{(Ser2P\ Total)^{Tau}}{(Ser2P\ Total)^{Ctrl}}\right) = RNAP\ II\ Pause\ Index\ (PI)$$

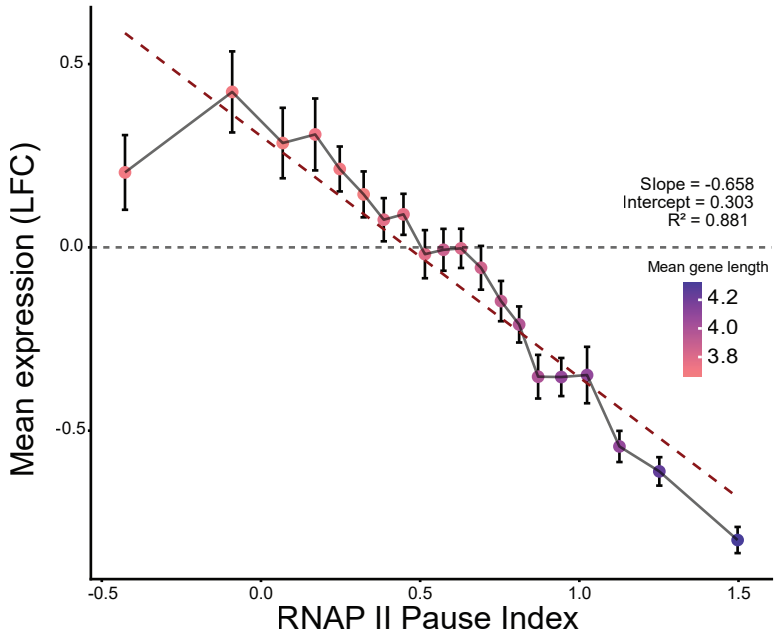

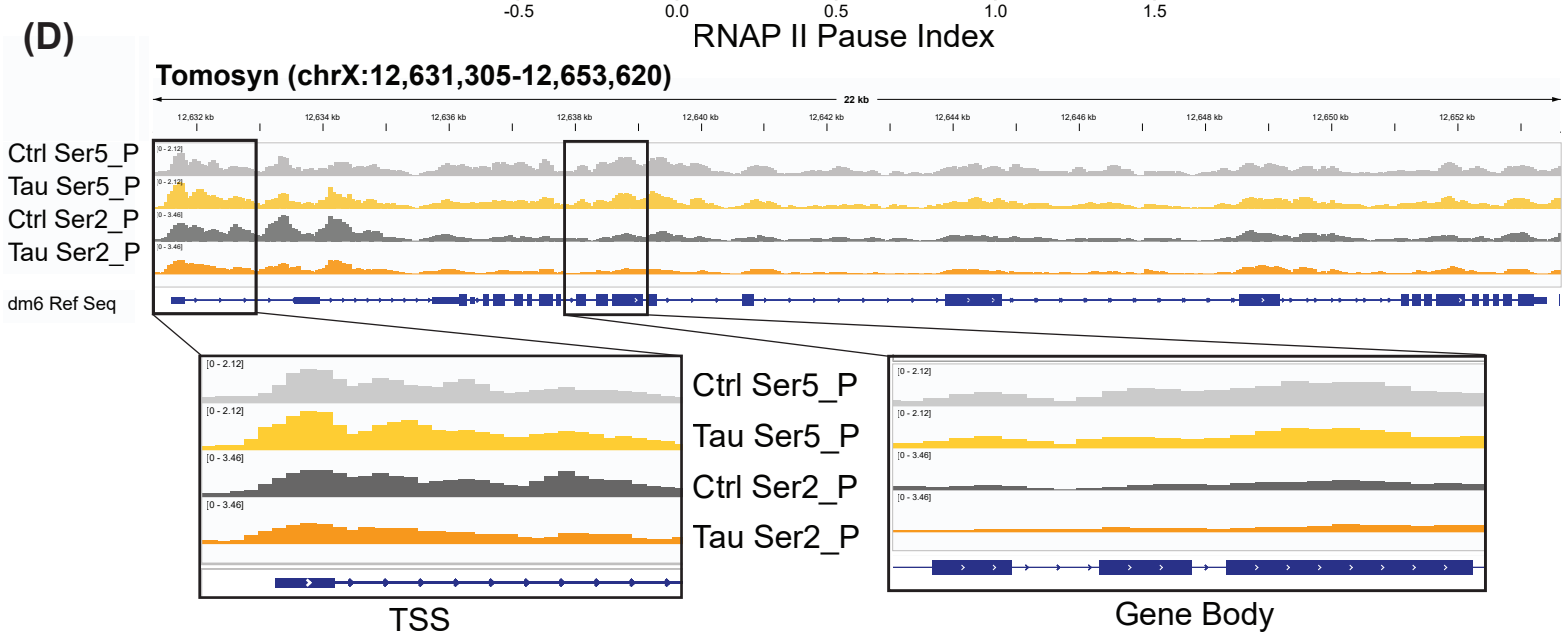

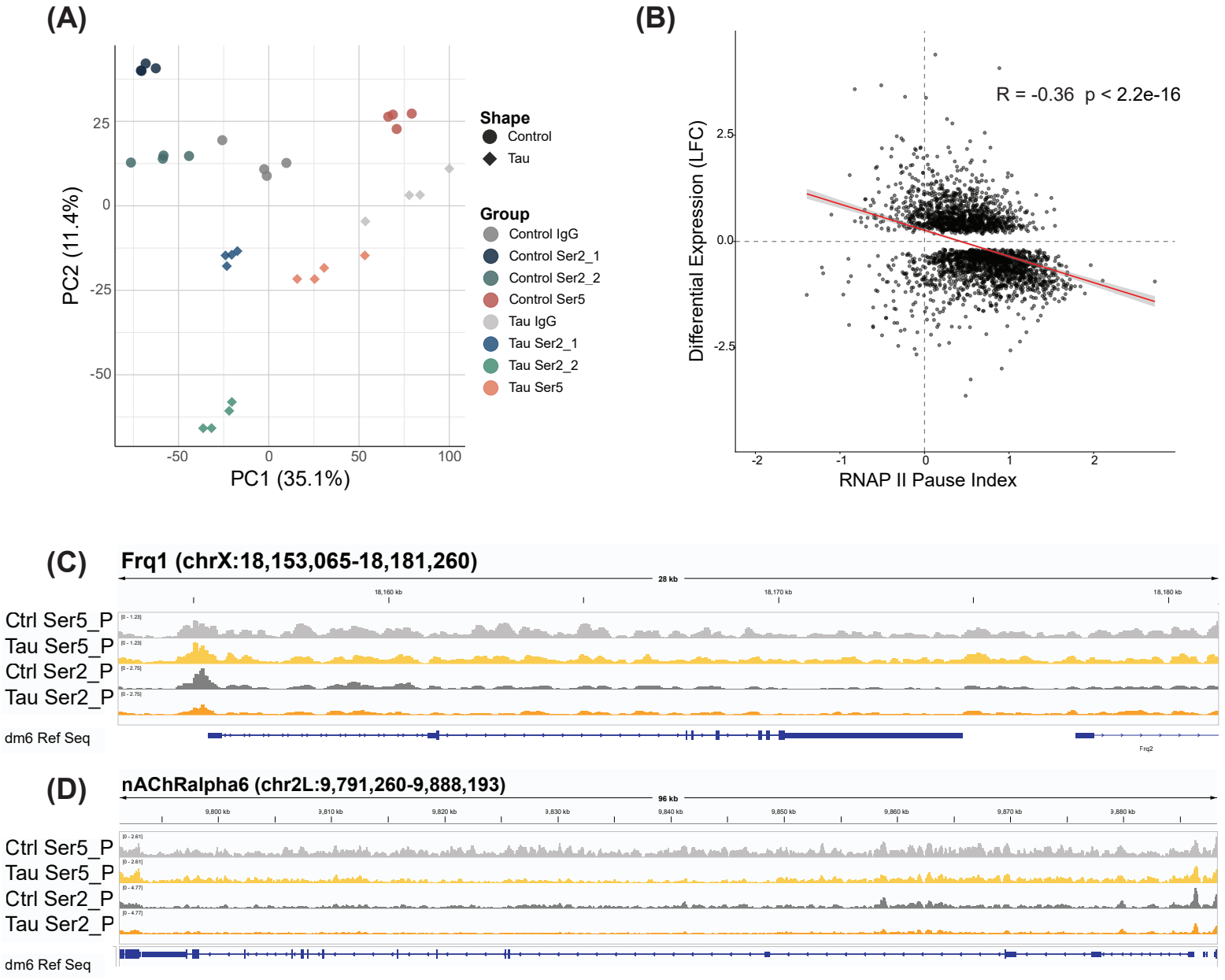
(A)
PC2 (11.4%)
PC1 (35.1%)
25
0
-25
-50
-50
0
50
100
Shape
Control
Tau
Group
Control IgG
Control Ser2_1
Control Ser2_2
Control Ser5
Tau IgG
Tau Ser2_1
Tau Ser2_2
Tau Ser5
(B)
R = -0.36 p < 2.2e-16
Differential Expression (LFC)
RNAP II Pause Index
2.5
0.0
-2.5
-2
-1
0
1
2
(C)
Frq1 (chrX:18,153,065-18,181,260)
28 kb
18,160 kb
18,170 kb
18,180 kb
Ctrl Ser5_P
Tau Ser5_P
Ctrl Ser2_P
Tau Ser2_P
dm6 Ref Seq
Frq2
(D)
nAChRalpha6 (chr2L:9,791,260-9,888,193)
96 kb
9,800 kb
9,810 kb
9,820 kb
9,830 kb
9,840 kb
9,850 kb
9,860 kb
9,870 kb
9,880 kb
Ctrl Ser5_P
Tau Ser5_P
Ctrl Ser2_P
Tau Ser2_P
dm6 Ref Seq